

1 **Lipopolysaccharide integrity primes bacterial sensitivity to a cell wall-degrading intermicrobial toxin**

2  
3 Kristine L Trotta<sup>1</sup>, Beth M Hayes<sup>1</sup>, Johannes P Schneider<sup>2</sup>, Jing Wang<sup>2</sup>, Horia Todor<sup>3</sup>, Patrick Rockefeller  
4 Grimes<sup>1</sup>, Ziyi Zhao<sup>1</sup>, William L Hatleberg<sup>4</sup>, Melanie R Silvis<sup>3</sup>, Rachel Kim<sup>1</sup>, Byoung Mo Koo<sup>3</sup>, Marek Basler<sup>2</sup>,  
5 Seemay Chou<sup>1\*</sup>

6  
7 <sup>1</sup> Department of Biochemistry & Biophysics, University of California – San Francisco, San Francisco, CA, USA

8 <sup>2</sup> Focal Area Infection Biology, Biozentrum, University of Basel, Klingelbergstrasse 50/70, CH - 4056

9 Basel, Switzerland

10 <sup>3</sup> Department of Cell and Tissue Biology, University of California – San Francisco, San Francisco, CA, USA

11 <sup>4</sup> Independent Researcher, Pittsburgh, Pennsylvania, USA

12  
13 \*Corresponding author: Seemay Chou (seemaychou@gmail.com)

14  
15 **ABSTRACT**

16  
17 Gram-negative bacteria can antagonize neighboring microbes using a type VI secretion system (T6SS) to deliver  
18 toxins that target different essential cellular features. Despite the conserved nature of these targets, T6SS  
19 potency can vary across recipient species. To understand the molecular basis of intrinsic T6SS susceptibility, we  
20 screened for essential *Escherichia coli* genes that affect its survival when antagonized by a cell wall-degrading  
21 T6SS toxin from *Pseudomonas aeruginosa*, Tae1. We revealed genes associated with both the cell wall and a  
22 separate layer of the cell envelope, surface lipopolysaccharide, that modulate Tae1 toxicity *in vivo*. Disruption of  
23 lipopolysaccharide synthesis provided *Escherichia coli* (*Eco*) with novel resistance to Tae1, despite significant cell  
24 wall degradation. These data suggest that Tae1 toxicity is determined not only by direct substrate damage, but  
25 also by indirect cell envelope homeostasis activities. We also found that Tae1-resistant *Eco* exhibited reduced cell  
26 wall synthesis and overall slowed growth, suggesting that reactive cell envelope maintenance pathways could  
27 promote, not prevent, self-lysis. Together, our study highlights the consequences of co-regulating essential  
28 pathways on recipient fitness during interbacterial competition, and how antibacterial toxins leverage cellular  
29 vulnerabilities that are both direct and indirect to their specific targets *in vivo*.

## 30 INTRODUCTION

31  
32 Many bacteria live in mixed-species microbial communities where they compete with each other for limited space  
33 and resources<sup>1</sup>. Intermicrobial competition is mediated by a diverse array of molecular strategies that can exclude  
34 or directly interfere with other microbes, both near and far<sup>2</sup>. Nearly 25% of Gram-negative bacteria encode a type  
35 VI secretion system (T6SS)<sup>3</sup>, which antagonizes neighboring cells by injection of toxic protein effectors into a  
36 recipient cell<sup>4-6</sup>. The opportunistic human pathogen *Pseudomonas aeruginosa* (*Pae*) harbors an interbacterial  
37 T6SS (H1-T6SS)<sup>7</sup> that can kill the model bacterium *Escherichia coli* (*Eco*)<sup>8-10</sup>. Studies of H1-T6SS-mediated  
38 competition between these genetically tractable species have provided fundamental insights into the molecular  
39 basis of T6SS function and regulation.

40  
41 Key to *Pae* H1-T6SS toxicity are its seven known effectors, each with a unique biochemical activity<sup>6,11-15</sup>. The T6S  
42 amidase effector 1 (Tae1) from *Pae* plays a dominant role in H1-T6SS-dependent killing of *Eco* by degrading  
43 peptidoglycan (PG), a structural component of the cell wall that is critical for managing cell shape and turgor<sup>16,17</sup>.  
44 Early efforts to understand Tae1 toxicity focused on its *in vitro* biochemical activity against PG, which offered key  
45 insights about how H1-T6SS targets select bacterial species. Tae1 specifically digests  $\gamma$ -D-glutamyl-meso-2,6-  
46 diaminopimelic acid (D-Glu-*m*DAP) peptide bonds, which are commonly found in PG from Gram-negative bacteria  
47 <sup>8,18</sup>. Tae1 toxicity is further restricted to non-kin cells through a *Pae* cognate immunity protein, T6S amidase  
48 immunity protein 1 (Tai1), which binds and inhibits Tae1 in kin cells<sup>11,19,20</sup>.

49  
50 However, biochemical specificity is not sufficient to explain the toxicity and organismal selectivity of T6SS  
51 effectors *in vivo*. Bacteria antagonized by T6SSs ('recipients') can actively regulate effector toxicity through  
52 adaptive stress responses. *Eco* upregulates its envelope stress responses Rcs and BaeSR after exposure to the  
53 *Vibrio cholerae* (V52) T6SS effectors TseH (a PG hydrolase)<sup>21</sup> and TseL (a lipase)<sup>22</sup>, suggesting that *Eco* could  
54 counter cell envelope damage by re-enforcing its surface<sup>23</sup>. Similarly, *Bacillus subtilis* triggers protective  
55 sporulation in response to a *Pseudomonas chlororaphis* (PCL1606) T6SS effector, Tse1 (a muramidase)<sup>24</sup>.  
56 Additional recipient-cell coordinators of T6SS effector toxicity include reactive oxygen species<sup>25</sup> and glucose-  
57 dependent gene expression<sup>26</sup>. These studies demonstrate that T6SS effector toxicity *in vivo* may also depend on  
58 downstream adaptive features of recipient cells.

59  
60 The cell wall is a complex and dynamic substrate that is actively regulated to protect the cell<sup>27-32</sup>, yet *Eco* is highly  
61 susceptible to lysis by Tae1 *in vivo*. We therefore hypothesized that Tae1 activity promotes H1-T6SS-mediated  
62 lysis in *Eco* through a unique strategy to overcome neutralization by the recipient cell. In this study, we  
63 investigated the *Eco* cellular features that drive its intrinsic sensitivity to H1-T6SS and the Tae1 toxin during  
64 interbacterial competition with *Pae*. Many T6SS effectors target essential cell features, so we screened the entire  
65 complement of essential *Eco* genes (plus some conditionally essential PG genes) for Tae1 susceptibility  
66 determinants. This approach complements previous genetic screens for T6SS recipient fitness which focused on  
67 nonessential gene candidates<sup>33,34</sup>. While cell wall-related genes indeed impacted *Eco* susceptibility to Tae1, we  
68 also discovered a strong relationship between survival and another component of the cell envelope,  
69 lipopolysaccharide (LPS). Perturbation of LPS synthesis genes *msbA* and *lpxK* rendered *Eco* conditionally  
70 resistant to lysis by Tae1 from *Pae*. Our work revealed that LPS-related resistance was mediated through cell-  
71 biological processes that were independent of the biochemical Tae1-PG interaction. Our findings suggest that  
72 beyond biochemical specificity and adaptive stress responses lies a role for essential homeostatic processes in  
73 defining T6SS effector toxicity *in vivo*.

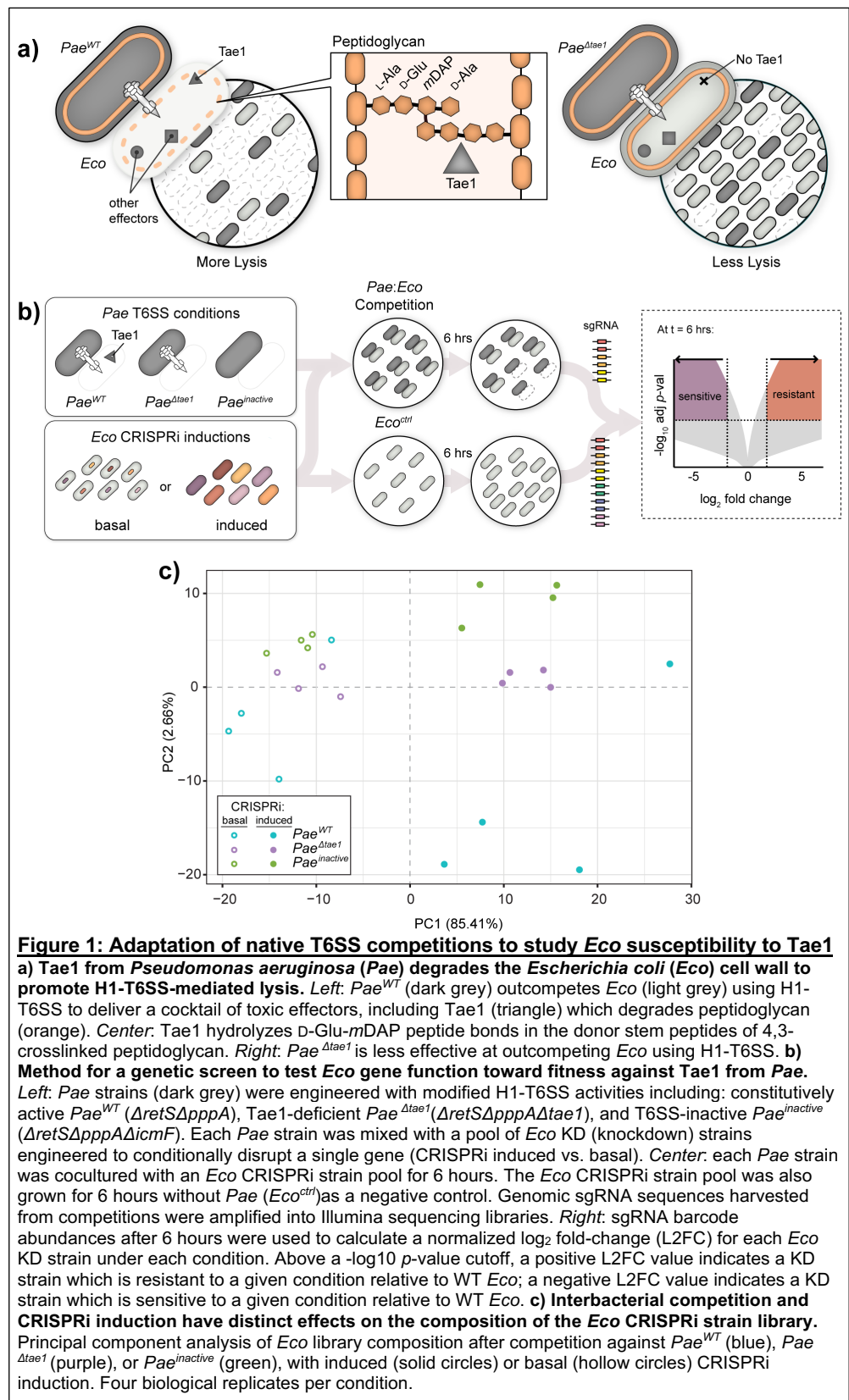
## 74 RESULTS

### 75 Adaptation of native T6SS competitions to study *Eco* susceptibility to Tae1

76  
77 We developed an *in vivo* screen for genetic interactions between the cell wall-degrading H1-T6SS effector Tae1  
78 from *Pae* and the model target bacterium *Eco*. Our screen had two fundamental design requirements: (1) the  
79 ability to distinguish between general (T6SS-dependent) and specific (Tae1-dependent) genetic interactions, and  
80 (2) the capacity to test a broad array of target cell features. We adapted an established interbacterial competition  
81 co-culture assay between H1-T6SS-active *Pae* and *Eco*, the outcome of which is sensitive to the specific  
82 contribution of Tae1<sup>8</sup>. In this assay *Eco* exhibits a greater fitness advantage when competed against *Pae* missing  
83 *tae1* (*Pae* <sup>$\Delta$ tae1</sup>) relative to an equivalent control strain (*Pae*<sup>WT</sup>) (**Figure 1a**). We hypothesized that the *Pae*:*Eco* co-  
84 culture assay could be leveraged to quantitatively compare recipient cell fitness against both Tae1 (toxin-specific  
85 fitness) and the H1-T6SS (Tae1-independent fitness) in interbacterial competition.  
86  
87  
88

89 To screen broadly for *Eco* determinants, we adopted an established *Eco* CRISPR interference (CRISPRi)  
 90 platform that generates hypomorphic mutants through intermediate gene expression knockdowns (KDs)<sup>35</sup>. In  
 91 contrast to knock-outs or transposon mutagenesis studies, CRISPRi is systematically amenable to essential  
 92 genes and thus provided an opportunity to make unique insights about genes that are typically challenging to  
 93 screen for. This includes many essential (or conditionally essential) genes related to peptidoglycan (PG)  
 94 metabolism, whose KDs  
 95 we predicted would impact  
 96 *Tae1* toxicity. In this  
 97 CRISPRi system, inducible  
 98 sgRNA expression is  
 99 coupled with constitutive  
 100 dCas9 expression to  
 101 conditionally repress  
 102 transcription at specific loci  
 103 with and without induction  
 104 (“induced” and “basal”  
 105 CRISPRi, respectively)  
 106 (Supplemental Figure 1a).  
 107 In total, our CRISPRi  
 108 collection was composed of  
 109 596 *Eco* strains with KDs  
 110 representing most cellular  
 111 functions as defined by the  
 112 NCBI clusters of  
 113 orthologous genes (COG)  
 114 system (Supp. Fig. 1b).  
 115 Our collection also included  
 116 50 negative control strains  
 117 with non-targeting sgRNAs,  
 118 including *rfp-KD*, to ensure  
 119 CRISPRi alone did not  
 120 impact inherent *Eco*  
 121 susceptibility to *Pae* (Supp.  
 122 Fig. 2a).

123  
 124 For the interbacterial  
 125 competition screen, we co-  
 126 cultured *Pae* with the  
 127 pooled *Eco* CRISPRi  
 128 collection to test  
 129 competitive fitness across  
 130 all KD strains in parallel  
 131 (Fig. 1b). To compare  
 132 *Tae1*-dependent and -  
 133 independent fitness  
 134 determinants, we  
 135 conducted screens against  
 136 H1-T6SS-active *Pae*  
 137 strains that either secrete  
 138 *Tae1* (*Pae*<sup>WT</sup>;  $\Delta retS\Delta pppA$ )  
 139 or are *Tae1*-deficient  
 140 (*Pae* <sup>$\Delta tae1$</sup> ;  
 141  $\Delta retS\Delta pppA\Delta tae1$ ). As  
 142 negative controls, we also  
 143 competed the *Eco*  
 144 collection against a  
 145 genetically H1-T6SS-  
 146 inactivated *Pae* strain  
 147 (*Pae*<sup>*inactive*</sup>;



148  $\Delta retS \Delta pppA \Delta icmF$ ) and included a condition in which the collection was grown without *Pae* present (*Eco<sup>ctrl</sup>*).  
 149 Experiments were performed under both induced and basal CRISPRi conditions to distinguish between general  
 150 *Eco* fitness changes and those due to transcriptional knockdown. We used high-throughput sequencing to  
 151 quantify KD strain abundance at the beginning and end of each six-hour competition. To understand the  
 152 contribution of each KD to *Eco* survival against *Pae* in the presence or absence of H1-T6SS or *Tae1*, we  
 153 calculated log<sub>2</sub> fold-change (L2FC) values for each KD strain after competition and normalized against abundance  
 154 after growth without competition (*Eco<sup>ctrl</sup>*)<sup>36,37</sup>. Across four biological replicates per condition, L2FC values were  
 155 reproducible (**Supp. Fig. 3a**; median Pearson's *r* between all replicates = 0.91). L2FC was used as a proxy for  
 156 competitive fitness of KD strains across different competition conditions.

157  
 158 To determine if our screen was sensitive to the effects of *Tae1*, H1-T6SS, and CRISPRi, we conducted a principal  
 159 component analysis of L2FC values for each strain under every competition condition (**Fig. 1c**). We observed  
 160 clear separation of datasets by CRISPRi induction (induced versus basal) across the first principal component  
 161 (PC1; 85.41%), indicating that KD induction was a major contributor to the performance of the KD library in the  
 162 pooled screen. We also observed clustering of datasets according to *Pae* competitor (PC2; 2.66%). These results  
 163 indicate that each *Pae* competitor yielded a distinct effect on the fitness of the CRISPRi library and demonstrates  
 164 that our screen was sensitive to the presence (*Pae<sup>WT</sup>*) or absence (*Pae<sup>Δtae1</sup>*) of *Tae1* delivery from H1-T6SS.  
 165 From these data we conclude that our screen successfully captured the unique impacts of CRISPRi, *Tae1*, and  
 166 H1-T6SS on pooled *Eco* CRISPRi libraries during interbacterial competition.

## 167 CRISPRi reveals toxin-specific and non-specific determinants of *Eco* fitness against H1-T6SS

168  
 169 To reveal specific *Eco* genes that shape intrinsic susceptibility to H1-T6SS-mediated antagonism, we identified  
 170 KD strains which were significantly depleted or enriched at least three-fold (L2FC < -1.585 for depletion or  
 171 L2FC > 1.585 for enrichment, and -log<sub>10</sub> p-adj < 0.05) after competition against *Pae<sup>WT</sup>*, *Pae<sup>Δtae1</sup>*, or *Pae<sup>inactive</sup>*. Our  
 172 goal was to prioritize KDs which had a unique effect on fitness against *Pae<sup>WT</sup>* relative to conditions lacking *Tae1*.  
 173 With CRISPRi induced, we found a select cohort of KDs with significant loss of fitness (*n*=12) or gain of fitness  
 174 (*n*=11) against *Pae<sup>WT</sup>* (**Fig. 2a**). We were surprised that some KDs caused resistance to *Tae1* despite the  
 175 combined challenge of essential gene depletion and H1-T6SS antagonism.

176  
 177 Competition against *Pae<sup>WT</sup>* with basal CRISPRi diminished the pool of significant candidate KDs (**Supp. 4a**),  
 178 reinforcing our observation that KD strains' fitness changes against *Pae* are dependent on CRISPRi induction.  
 179 Against *Pae<sup>Δtae1</sup>* (CRISPRi induced), we observed seventeen KDs with significant fitness changes (**Fig. 2b**) which  
 180 were also CRISPRi-dependent (**Supp. 4b**). These KDs were mostly distinct from those that affected *Eco* fitness  
 181 against *Pae<sup>WT</sup>* (**Fig. 2c**). These results indicate that the presence or absence of *Tae1* had a unique effect on the  
 182 T6SS competition and thus had a distinct impact on KD fitness. Finally, we found few candidate KDs that affected  
 183

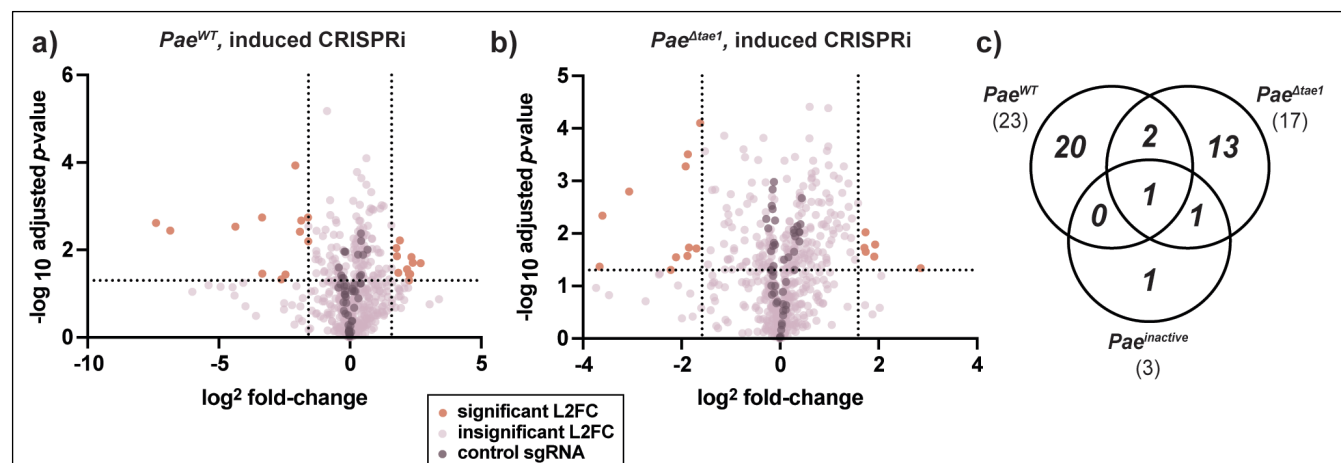


**Figure 2: CRISPRi reveals toxin-specific and non-specific determinants of *Eco* fitness against H1-T6SS**

**a-b** CRISPRi knockdowns promote *Eco* survival against *Pae<sup>WT</sup>* (a) and *Pae<sup>Δtae1</sup>* (b). Volcano plots showing log<sub>2</sub>-fold change (L2FC) values for each KD strain after interbacterial competition (induced CRISPRi). Data shown: mean from four biological replicates. Statistical test: Wald test. Vertical dotted lines indicate arbitrary cutoffs for L2FC at *x* = -1.58 and *x* = 1.58 (absolute FC *x* = 3 or *x* = 3). Horizontal dotted line indicates statistical significance cutoff for log<sub>10</sub> adjusted p-value (≤ 0.05). Orange points represent KDs with L2FC ≥ 1.58 or ≤ -1.58 and log<sub>10</sub>-adj. *p*-value ≤ 0.05. Dark purple points represent non-targeting negative control KDs (*n*=50). Lavender points represent KDs that do not meet cutoffs for L2FC or statistical test. **c** T6SS competitions identify CRISPRi strains with distinct fitness changes against T6SS and *Tae1*. Venn diagram of total KDs significantly enriched OR depleted after competition against *Pae<sup>WT</sup>* (*n*=23), *Pae<sup>Δtae1</sup>* (*n*=17), and *Pae<sup>inactive</sup>* (*n*=5).



184 fitness against *Pae*<sup>inactive</sup> regardless  
 185 of CRISPRi induction condition  
 186 (Supp. 4a-b), suggesting that most  
 187 significant phenotypes were H1-  
 188 T6SS-dependent, if not Tae1-  
 189 dependent. In fact, L2FC values in  
 190 *Pae*<sup>inactive</sup> and *Eco*<sup>ctrl</sup> datasets had  
 191 high correlation (Supp. 4 c-d,  
 192 median Pearson correlation  $r=$   
 193 0.98), indicating that *Pae* is a  
 194 neutral co-culture partner with its  
 195 H1-T6SS inactivated.  
 196 With our interest in Tae1-specific  
 197 determinants, we focused our  
 198 attention on the 20 KDs which had  
 199 a unique effect on *Eco* fitness  
 200 against Tae1 (*Pae*<sup>WT</sup>+CRISPRi  
 201 induced; Table 1). Most KDs in this  
 202 group targeted genes related to the  
 203 cell envelope (COG category M:  
 204 cell wall/membrane/envelope  
 205 biogenesis,  $n=13/20$ ). Composed  
 206 of concentric layers of inner  
 207 membrane (IM), cell wall PG, outer  
 208 membrane (OM), and  
 209 lipopolysaccharide (LPS)<sup>38</sup>(Fig.  
 210 3b), the cell envelope is a critical  
 211 structure for protecting *Eco* against  
 212 environmental stress. Tae1-  
 213 sensitized strains were dominated  
 214 by gene targets related to the  
 215 synthesis of PG (*murA*, *ftsI*, *murC*,  
 216 *murI*, *mcrB*, *murJ*). Given that Tae1  
 217 targets the cell wall, these results  
 218 support our initial hypothesis that  
 219 PG structural integrity or  
 220 composition are direct  
 221 determinants of Tae1 susceptibility.

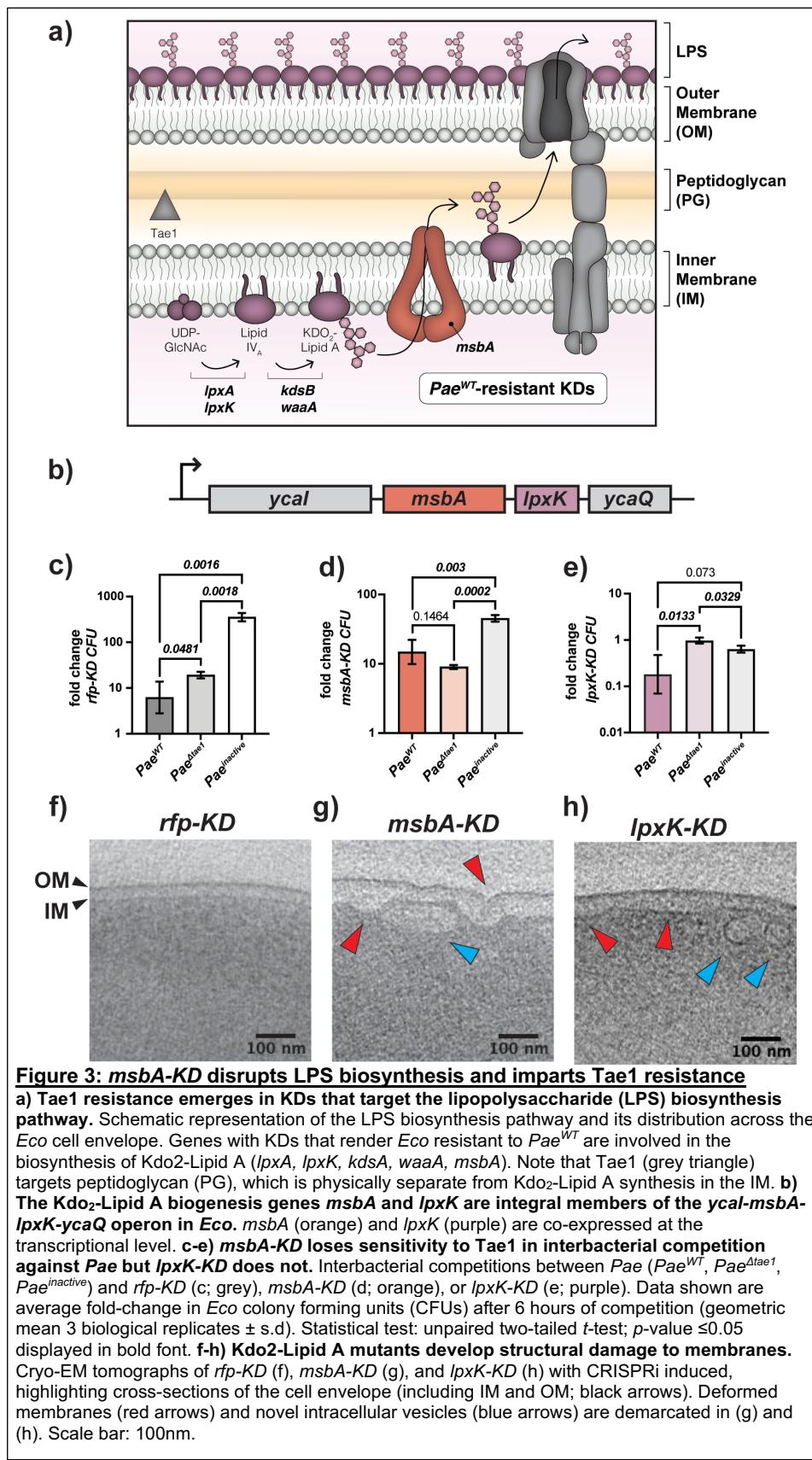
222 KDs related to lipid membrane metabolism and transport offered either resistance (*pssA*, *acpP*, *ffs*, *ffh*) or  
 223 sensitivity (*accD*, *bamA*) to Tae1, indicating that cell envelope factors indirect to the effector-substrate interaction  
 224 could impact Tae1 toxicity. To our surprise, most KDs that rendered *Eco* resistant to *Pae*<sup>WT</sup> were related to LPS  
 225 synthesis and transport. Tae1 is not known to directly interact with the IM, OM, or LPS as part of its molecular  
 226 mechanism but metabolic crosstalk does occur between the PG, LPS, and lipid biosynthesis pathways<sup>31,39</sup>. Thus,  
 227 our data raised the possibility that regulation of other cell envelope structures could also be implicated in  
 228 mediating cell wall attack.

### 230 *msbA*-KD disrupts LPS biosynthesis and imparts Tae1 resistance

232 To investigate the hypothesis that non-PG components of the cell envelope may also shape Tae1 toxicity, we  
 233 focused downstream studies on Tae1-resistant KDs related to the synthesis of LPS, an essential lipidated surface  
 234 sugar that offers protection and structure to the OM<sup>40</sup>. Candidate KDs targeted highly-conserved, essential genes  
 235 in Kdo<sub>2</sub>-Lipid A synthesis and transport (*lpxA*, *lpxK*, *kdsB*, *waaA*, *msbA*) (Fig. 3a). Kdo<sub>2</sub>-Lipid A synthesis is the  
 236 most-upstream arm of LPS biosynthesis with rate-limiting control over the entire pathway<sup>41,42</sup>. In our screen, the  
 237 strongest resistance phenotypes we observed were in KDs targeting *lpxK* (*lpxK\_-1as* and *lpxK\_32as*) (Table 1).  
 238 LpxK is a kinase that phosphorylates the Lipid-A intermediate tetraacyldisaccharide 1-phosphate to form Lipid  
 239 IV<sub>A</sub><sup>43,44</sup>. In *Eco*, *lpxK* is in an operon with *msbA* (Fig. 3b), which encodes the IM Kdo<sub>2</sub>-Lipid A flippase MsbA<sup>45,46</sup>. A  
 240 KD of *msbA* (*msbA\_40as*) also conferred resistance to *Pae*<sup>WT</sup> in our screen (Table 1).  
 241

KD target	pathway/process	Avg. L2FC ( <i>Pae</i> <sup>WT</sup> )	fitness against <i>Pae</i> <sup>WT</sup>
<i>murA</i>	PG synthesis	-7.40	sensitive
<i>ftsI</i>	Cell division	-6.85	sensitive
<i>accD</i>	Lipid metabolism	-4.37	sensitive
<i>lptC</i>	LPS transport	-3.35	sensitive
<i>murC</i>	PG synthesis	-2.61	sensitive
<i>bamA</i>	OM protein assembly	-2.46	sensitive
<i>murI</i>	PG synthesis	-1.86	sensitive
<i>mrcB</i>	PG synthesis	-1.60	sensitive
<i>murJ</i>	PG transport	-1.59	sensitive
<i>pssA</i>	Lipid metabolism	1.77	resistant
<i>hemE</i>	Heme metabolism	1.79	resistant
<i>msbA</i>	LPS transport	1.84	resistant
<i>waaA</i>	LPS synthesis	1.91	resistant
<i>lpxA</i>	LPS synthesis	2.18	resistant
<i>ffs</i>	Membrane trafficking/ secretion	2.25	resistant
<i>acpP</i>	Lipid metabolism	2.25	resistant
<i>ffh</i>	Membrane trafficking/ secretion	2.30	resistant
<i>kdsB</i>	LPS synthesis	2.35	resistant
<i>lpxK (lpxK_-1as)</i>	LPS synthesis	2.39	resistant
<i>lpxK (lpxK_32as)</i>	LPS synthesis	2.69	resistant

**Table 1: Cell envelope gene KDs develop strong fitness changes against Tae1 in competition.** KDs that target PG synthesis can increase *Pae*<sup>WT</sup> sensitivity, while targeting other cell envelope processes can result in sensitivity or resistance. Data shown: normalized L2FC values for all 20 KD strains with unique and significant fitness changes against *Pae*<sup>WT</sup> (which secretes Tae1); average of four biological replicates.



We first experimentally validated pooled screen results by individually testing *lpxK*-KD and *msbA*-KD fitness in binary competitions against *Pae*. We regenerated and validated KD strains for *lpxK* (*lpxK*<sub>-1as</sub>; “*lpxK*-KD”) and *msbA* (“*msbA*-KD”) for use in these experiments (Supp. 6). Consistent with our screen, *msbA*-KD gained *Tae1*-specific resistance in H1-T6SS-mediated competitions (Fig. 3d), exhibiting loss of sensitivity to *Pae*<sup>WT</sup> relative to *Pae*<sup>Δtae1</sup>. In contrast, we could not validate *Tae1* resistance for *lpxK*-KD (Fig. 3e). Like *rfp*-KD (Fig. 3c), *lpxK*-KD maintains sensitivity to *Pae*<sup>WT</sup> relative to *Pae*<sup>Δtae1</sup>. The gene expression of *msbA* and *lpxK* are co-dependent, so we were surprised that *msbA*-KD and *lpxK*-KD did not equally reproduce *Tae1* resistance. However, CRISPRi-dependent phenotypes could be controlled by factors such as transcriptional polar effects or off-target CRISPRi effects. To address their phenotypic disparities, we quantified transcriptional KD efficacy and specificity for *lpxK*-KD and *msbA*-KD with qRT-PCR. For *msbA*-KD with CRISPRi induced, we found repression of *msbA* (29-fold), *lpxK* (15-fold), and *ycaQ* (3.6-fold) expression (Supp. Fig. 6a). Thus, owing to downstream polar effects, our *msbA*-KD strain is a KD of both LPS candidate genes, *msbA* and *lpxK*. Conversely, *lpxK*-KD only repressed *lpxK* (71-fold) and *ycaQ* (11-fold) (Supp. Fig. 6b), but not *msbA*. Therefore, *msbA*-KD and *lpxK*-KD yield distinct transcriptional consequences despite targeting the same operon using CRISPRi.

298 Next, we investigated phenotypic consequences of inducing CRISPRi in *msbA*-KD and *lpxK*-KD by comparing  
 299 their cellular morphologies with cryo-electron tomography. Disruption of *msbA* and *lpxK* typically leads to  
 300 structural deformation in the *Eco* cell envelope from aberrant accumulation of Kdo<sub>2</sub>-Lipid A intermediates in the

301 IM<sup>44,46,47</sup>. Unlike *rfp-KD* negative control cells (**Fig. 3e**), *msbA-KD* cells developed irregular buckling in the IM and  
 302 OM (**Fig. 3f**, red arrows). We also observed vesicular or tubular membrane structures within the cytoplasm (**Fig.**  
 303 **3f**, blue arrows). Such structural abnormalities are consistent with physical crowding of Kdo<sub>2</sub>-Lipid A intermediates  
 304 in the IM that are relieved by vesicular internalization. On the other hand, while *lpxK-KD* had a distended IM and  
 305 vesicles (**Fig. 3g**, red and blue arrows), the OM appeared smooth and regular. This phenotypic divergence points  
 306 to two distinct KD effects: defects in the IM (both *msbA-KD* and *lpxK-KD*) and defects in the OM (*msbA-KD* only).  
 307 Together with our transcriptional analyses, these results demonstrate that *msbA-KD* and *lpxK-KD* have unique  
 308 consequences for LPS integrity and Tae1 susceptibility despite targeting the same operon. We focused the  
 309 remainder of our study on the validated *msbA-KD* strain which damages the IM and OM.

## 311 Resistance to Tae1 in *msbA-KD* is independent of cell wall hydrolysis

312 Identifying *msbA* and *lpxK* as potential Tae1 resistance determinants provided us a chance to study mechanisms  
 313 by which LPS impacts

314 susceptibility to cell wall  
 315 damage. Such mechanisms  
 316 could span several scales  
 317 including: direct Tae1-PG  
 318 interactions (**Fig. 4**), cellular  
 319 responses to Tae1 hydrolysis  
 320 (**Fig. 5**), broad physiological  
 321 conditions that affect  
 322 mechanical lysis (**Fig. 6**), or  
 323 some combination of these. To  
 324 investigate, we used an  
 325 orthogonal *in vivo* assay to  
 326 directly test the effect of Tae1  
 327 activity in *msbA-KD* cells in the  
 328 absence of *Pae* and other co-  
 329 delivered H1-T6SS toxins. We  
 330 measured lysis for *rfp-KD* and  
 331 *msbA-KD* upon induction of  
 332 exogenous wild-type Tae1  
 333 (Tae1<sup>WT</sup>) expression in the cell  
 334 wall-containing periplasm<sup>8,48</sup> and  
 335 found that *msbA-KD* had  
 336 increased survival against  
 337 Tae1<sup>WT</sup> relative to *rfp-KD* (**Fig.**  
 338 **4a**). *Eco* resistance was  
 339 dependent on Tae1 activity, as  
 340 evidenced by loss of the *msbA-*  
 341 *KD* resistance phenotype with  
 342 catalytically-attenuated  
 343 Tae1<sup>C30A</sup> (**Fig. 4b**) and no-  
 344 enzyme (empty) (**Fig. 4c**)  
 345 controls. There were no major  
 346 differences in Tae1 expression  
 347 levels across conditions (**Supp.**  
 348 **Fig. 7a-b**), which ruled out the  
 349 possibility that fitness was tied  
 350 to toxin dose. Complementation  
 351 of *msbA* by overexpression  
 352 partially rescued Tae1<sup>WT</sup>  
 353 susceptibility in *msbA-KD*  
 354 (**Supp. Fig. 8a-c,g**), while *lpxK*  
 355 overexpression did not (**Supp.**  
 356 **Fig. 8d-f,h**). Given the  
 357 multigenic knockdown in *msbA-*  
 358

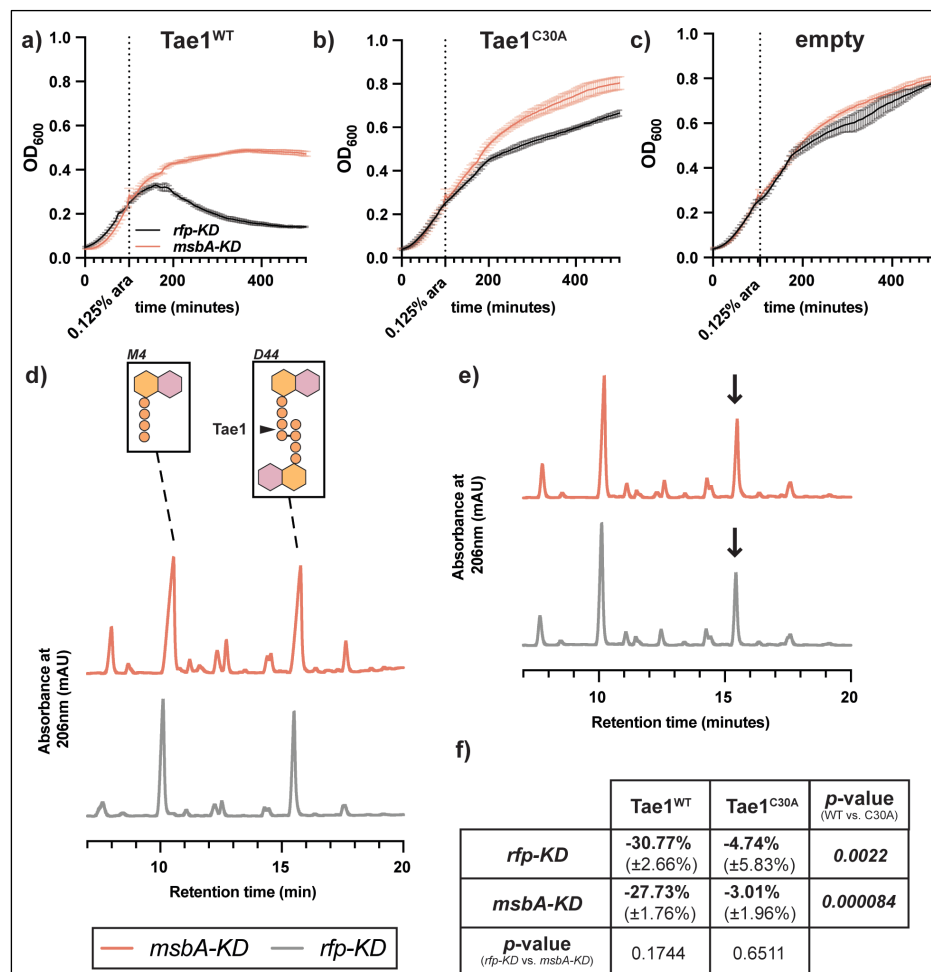


**Figure 4: Resistance to Tae1 in *msbA-KD* is independent of cell wall hydrolysis**  
**a-c) *msbA-KD* populations have a Tae1-dependent growth advantage.** OD<sub>600</sub> growth curves of *msbA-KD* (orange) and *rfp-KD* (black) with CRISPRi induced, overexpressing (a) *pBAD24::pelB-tae1<sup>WT</sup>* (Tae1<sup>WT</sup>), (b) *pBAD24::pelB-tae1<sup>C30A</sup>* (Tae1<sup>C30A</sup>), or (c) *pBAD24* (empty). Data shown: average of 3 biological replicates ± s.d. Dotted vertical line indicates plasmid induction timepoint (at OD<sub>600</sub>=0.25). **d) The mucopeptide composition of *msbA-KD* PG is identical to control *rfp-KD*.** HPLC chromatograms of mucopeptides purified from *msbA-KD* (orange) and *rfp-KD* (grey) expressing *pBAD24* (empty). Inset: major mucopeptide species in *Eco* include tetrapeptide monomers (M4; r.t. ~10 minutes) and 4,3-crosslinked tetra-tetra dimers (D44; r.t. ~15.5 minutes). Tae1 digests D44 peptides (black arrow). Data shown: representative from 3 biological replicates. **e) Tae1<sup>WT</sup> digests PG from both *msbA-KD* and *rfp-KD* PG *in vivo*.** HPLC chromatograms of mucopeptides purified from *msbA-KD* (orange) and *rfp-KD* (grey) expressing *pBAD24::pelB-tae1<sup>WT</sup>* (Tae1<sup>WT</sup>). Black arrow indicates D44 peptide partially digested by Tae1. Data shown: representative from 3 biological replicates. **f) Tae1 is equally efficient at digesting PG in *msbA-KD* and *rfp-KD*.** Percent loss of D44 peptide after 60 minutes of periplasmic Tae1<sup>WT</sup> or Tae1<sup>C30A</sup> expression. Data shown: average of 3 biological replicates (± s.d.). Statistical test: two-tailed unpaired *t*-test; p-value ≤ 0.05 displayed in bold font.



359 *lpxK-ycaQ* in *msbA-KD*, these data suggest that *msbA* is a partial determinant of Tae1 susceptibility in the strain.

360  
361 Next, we tested whether *msbA-KD* directly impacts Tae1–PG physical interactions by triggering changes to the  
362 chemical composition of *Eco* PG, which can occur downstream of OM stress<sup>31</sup>. PG remodeling could alter intrinsic  
363 Tae1 susceptibility by changing the relative abundance of targetable peptides in the cell wall. We isolated and  
364 characterized the composition of PG purified from *rfp-KD* and *msbA-KD* by HPLC muropeptide analysis. Both  
365 strains had highly similar and stereotypical *Eco* muropeptide profiles (Fig. 4d). PG peptides containing the scissile  
366 bond and structural context for Tae1 recognition (4,3-crosslinked dimers; D44)<sup>8</sup> were found at an approximate 1:1  
367 ratio with another dominant species of muropeptide (tetrapeptide monomers; M4)<sup>49</sup>. Our results suggest that the  
368 PG composition of *msbA-KD* is not modified downstream  
369 of LPS damage, indicating that Tae1 resistance cannot be  
370 explained by biochemical changes to the Tae1:PG  
371 interaction.

372  
373 We tested an alternative hypothesis that resistance may  
374 derive from decreased efficiency in Tae1 hydrolysis. We  
375 reasoned that structural deformations in the *msbA-KD* cell  
376 envelope (Fig. 3f) could occlude or delay the accessibility  
377 of PG to Tae1, thus slowing the kinetics of cell wall  
378 degradation and cell lysis. To test this, we monitored the  
379 relative degradation of D44 peptides after Tae1 induction  
380 in *rfp-KD* and *msbA-KD* populations. Empty-vector and  
381 Tae1<sup>C30A</sup> conditions were included as negative controls  
382 (Fig4d,f; Supp. Fig. 9a). At 60 minutes of induction (just  
383 prior to lysis in *rfp-KD* populations), we found that D44  
384 peptides were similarly hydrolyzed between strains, with a  
385 32.58% loss in *rfp-KD* and 27.73% of in *msbA-KD* (Fig.  
386 4e-f). Thus, Tae1 hydrolyzes *msbA-KD* PG as efficiently  
387 as *rfp-KD* PG. Collectively, these data show that both cell  
388 wall recognition and hydrolysis by Tae1 are unchanged in  
389 *msbA-KD*, ruling out the possibility that direct changes to  
390 PG are responsible for differential cellular lysis outcomes.

### 391 392 **PG synthesis is suppressed in *msbA-KD* but sensitive to Tae1 activity**

393  
394 Given that we did not find any effects on direct Tae1–cell  
395 wall interactions in *msbA-KD*, we next explored indirect  
396 resistance mechanisms. The PG sacculus is dynamically  
397 synthesized, edited, and recycled *in vivo* to maintain  
398 mechanical support to the cell during growth and  
399 stress<sup>27,50</sup>. We hypothesized that Tae1 hydrolysis could  
400 also impact PG synthesis activity in *Eco* by generating a  
401 need to replace damaged PG with new substrate. The  
402 ability to repair PG could thus be a valuable determinant  
403 of Tae1 susceptibility. To determine if PG synthesis is  
404 sensitive to Tae1 exposure, we measured the  
405 incorporation of the fluorescent D-amino acid HADA into  
406 *rfp-KD* cell walls both with and without exogenous Tae1  
407 expression. When normalized against control cells  
408 (*empty*), PG synthesis in *rfp-KD* cells increased by 22% in  
409 response to Tae1<sup>WT</sup> and decreased by 6.5% in response  
410 to Tae1<sup>C30A</sup> (Fig. 5a; Table 2). These data show that PG  
411 synthesis is stimulated by Tae1 exposure, and this response is dependent on toxin activity.

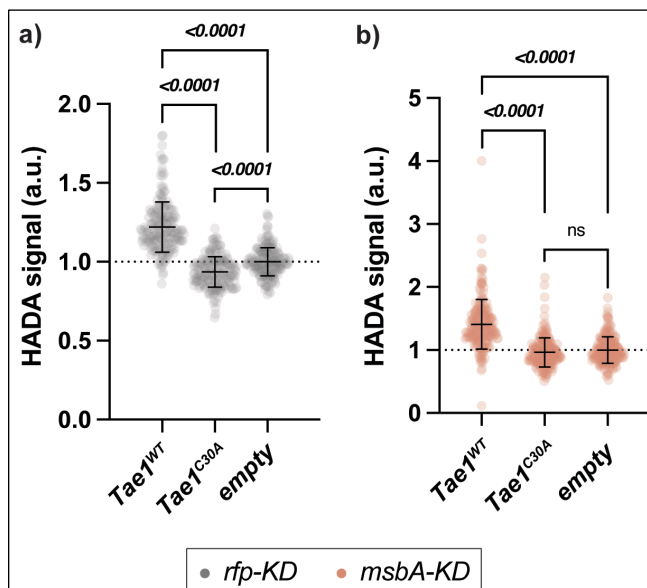


**Figure 5: PG synthesis is suppressed in *msbA-KD* but sensitive to Tae1 activity**

**a-b) PG synthesis activity is sensitive to Tae1 overexpression.** Single-cell fluorescence intensity measurements for *rfp-KD* (a; grey) or *msbA-KD* (b; orange) after incorporating the fluorescent D-amino acid HADA into PG after 60 minutes of overexpressing *pBAD24::pelB-tae1<sup>WT</sup>* (Tae1<sup>WT</sup>), *pBAD24::pelB-tae1<sup>C30A</sup>* (Tae1<sup>C30A</sup>), or *pBAD24* (*empty*), with CRISPRi induced. Data shown: 600 cells (200 cells x 3 biological replicates), with average ± s.d. Statistical test: unpaired two-tailed *t*-test; *p*-value ≤ 0.05 displayed in bold font.

		% change (intra-strain)	% change ( <i>rfp-KD</i> norm.)
<i>rfp-KD</i>	<b>Tae1<sup>WT</sup></b>	<b>22%</b> (±3.6%)	
	<b>Tae1<sup>C30A</sup></b>	<b>-6.5%</b> (±2.6%)	
	<b>empty</b>	<b>0%</b> (±1.6%)	
<i>msbA-KD</i>	<b>Tae1<sup>WT</sup></b>	<b>26.5%</b> (±2.5%)	<b>12%</b> (±2.5%)
	<b>Tae1<sup>C30A</sup></b>	<b>2.82%</b> (±3.2%)	<b>-9%</b> (±3.2%)
	<b>empty</b>	<b>0%</b> (±2.0%)	<b>-11.5%</b> (±2.0%)

**Table 2: PG synthesis activity is sensitive to CRISPRi and Tae1 overexpression.** Descriptive statistics for normalized percent change in HADA fluorescence in *rfp-KD* and *msbA-KD* as related to Fig.5 and Supp. Fig. 10. Data shown: average of 600 single-cell measurements ± s.d.



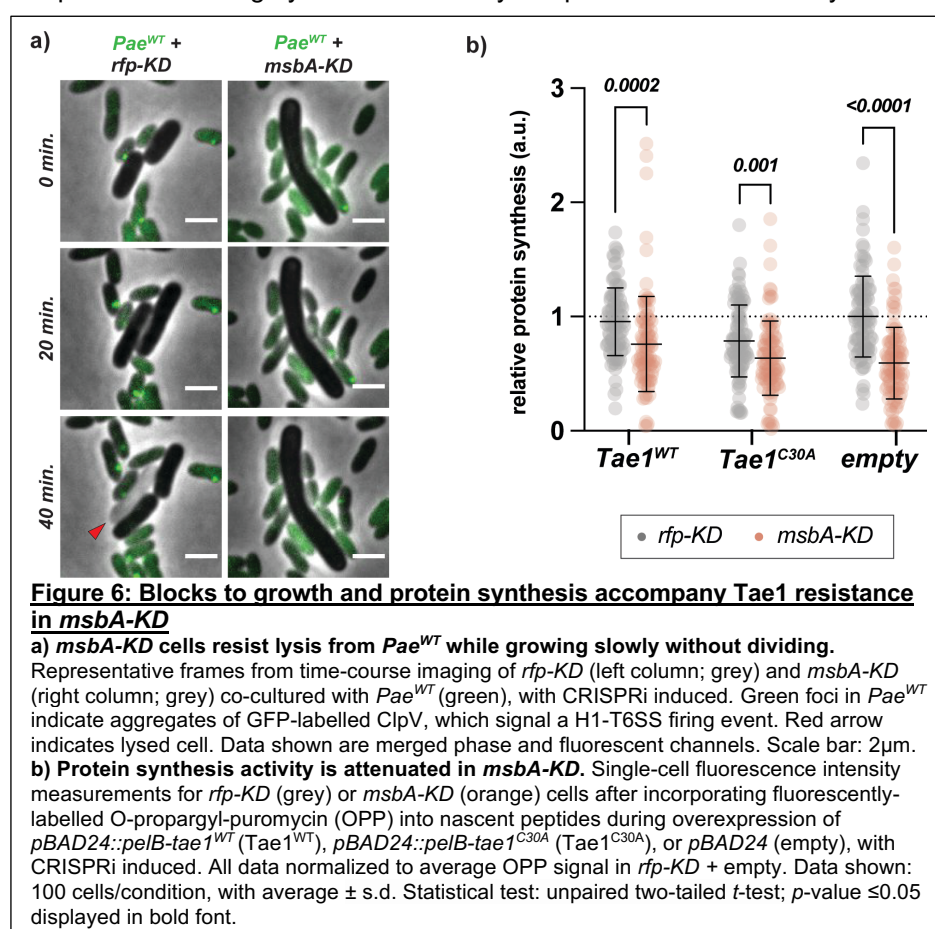
413 PG synthesis is also coordinated to other essential processes in *Eco*, and sensitive to their genetic or chemical  
 414 perturbations<sup>31,51</sup>. We investigated if *msbA-KD* impacts the dynamic PG synthesis response to Tae1. Tae1<sup>WT</sup>  
 415 exposure yielded a 26.5% increase in PG activity in *msbA-KD*, and no significant change in activity with Tae1<sup>C30A</sup>  
 416 (Fig. 5b; Table 2). These results indicate that PG synthesis is still actively regulated in *msbA-KD* in accordance  
 417 with relative Tae1 activity. However, when normalized against baseline *rfp-KD* activity, all PG synthesis  
 418 measurements for *msbA-KD* were significantly diminished (Supp. Fig. 10; Table 2). This observation indicates  
 419 that PG synthesis activity is globally suppressed as a consequence of CRISPRi in *msbA*. Thus, we conclude that  
 420 PG dynamism in *Eco* is sensitive to Tae1 hydrolysis of PG, and that *msbA-KD* alters the global capacity for PG  
 421 synthesis activity without altering its sensitivity to Tae1. Furthermore, these data suggest a reactive crosstalk  
 422 between LPS and PG synthesis activities *in vivo*.  
 423

### 424 Blocks to growth and protein synthesis accompany Tae1 resistance in *msbA-KD*

425  
 426 Based on its responsiveness to Tae1 exposure, we might hypothesize that *Eco* stimulates PG synthesis to  
 427 attempt protection against lysis by Tae1. However, suppressed PG synthesis activity alongside tolerance to  
 428 wildtype-levels of PG damage in *msbA-KD* suggested that *msbA-KD* may survive lysis by Tae1 using an  
 429 additional strategy to support or even supersede PG integrity. *Eco* can resist lysis upon acute PG stress by  
 430 transiently arresting homeostatic  
 431 functions like cell division, DNA  
 432 replication, and protein synthesis  
 433 to prioritize stress responses to  
 434 critical damage<sup>52-54</sup>. A recent  
 435 study showed that a CRISPRi KD  
 436 in *lpxA*, the first enzyme in Lipid A  
 437 biosynthesis, triggered hallmark  
 438 signs of a dormancy stress  
 439 response called the stringent  
 440 response<sup>55</sup>. Thus, we  
 441 hypothesized that decreased PG  
 442 synthesis activity in *msbA-KD*  
 443 may be symptomatic of a general,  
 444 KD-dependent slow growth  
 445 phenotype which could protect  
 446 against Tae1 activity by passive  
 447 tolerance.  
 448

449 To observe the effects of Tae1  
 450 and CRISPRi on cellular growth  
 451 and lysis behaviors over time, we  
 452 performed timelapse microscopy  
 453 of *rfp-KD* and *msbA-KD* cells in  
 454 competition with *Pae*. Across all  
 455 *Pae* competitions, *msbA-KD* cells  
 456 grew slowly without dividing or  
 457 lysing (Fig. 6a; Supp. Fig. 11a-  
 458 b). By contrast, *rfp-KD* cells grew  
 459 and divided rapidly, but lysed  
 460 when in competition against *Pae*  
 461 strains with active H1-T6SSs (*Pae*<sup>WT</sup>, *Pae*<sup>Δtae1</sup>) (Fig. 6a; Supp. Fig. 11a-b). These data demonstrate that stunted  
 462 cell growth and division are additional consequences of CRISPRi in *msbA-KD*. We orthogonally tested the effect  
 463 of *msbA-KD* on global cell physiology by measuring nascent protein synthesis activity in *msbA-KD* and *rfp-KD*.  
 464 Overall protein synthesis levels were significantly lower in *msbA-KD* relative to *rfp-KD* under all conditions tested  
 465 (Fig. 6a). From these data we conclude that *msbA-KD* cells exhibit broad changes in cellular physiology that may  
 466 underscore their unique ability to survive PG damage by Tae1.  
 467

468 We propose a model in which Tae1 susceptibility *in vivo* is determined at multiple levels of specificity in *Eco*: not  
 469 only at the level of local PG damage but also by crosstalk between essential cell envelope pathways and the  
 470 general growth state of the cell. As mediated through damage to LPS in *msbA-KD*, we posit that such crosstalk  
 471 between essential cell functions can be helpful for slowing reactivity and thus increasing tolerance to acute PG



472 stress. By the same token, the enmeshment of essential pathways may render fast-growing *Eco* vulnerable to  
473 Tae1 by creating a sudden chain-reaction of imbalances in critical functions which the cell must also resolve  
474 alongside the initial PG damage.

## 475 476 DISCUSSION

477  
478 The species composition of mixed-microbial communities can be driven by competitive strategies that bacteria  
479 use to antagonize their neighbors. However, our understanding of microbial weapons is primarily derived from *in*  
480 *vitro* studies of their molecular mechanisms. In this study, we wanted to understand how Tae1, a PG-degrading  
481 H1-T6SS effector toxin, specifically aided *Pae* in antagonizing *Eco in vivo*. By combining T6SS-mediated  
482 competition with CRISPRi against essential *Eco* genes, our high-throughput genetic screen was poised to  
483 uncover new molecular details about the interaction between Tae1 and essential functions in recipient cells.  
484 Related studies have successfully identified roles for nonessential genes that contribute to recipient survival  
485 against individual T6SS effectors<sup>33,34</sup>. Our study expands our understanding of intrinsic fitness against T6SS  
486 effectors by demonstrating how essential, homeostatic cell activities can have both direct (PG) and indirect (LPS,  
487 growth) impact on the effector-substrate interaction *in vivo*. We find that Tae1 toxicity is driven not only by its  
488 ability to destroy PG but also by broader physiological and regulatory contexts.

489  
490 Through the lens of LPS perturbation (*msbA-KD*), we discovered that slowing cell growth is associated with  
491 resistance to Tae1-dependent lysis. The protective nature of abject dormancy has been demonstrated for survival  
492 against other cell wall-degrading enzymes, lytic bacteriophages, and antibiotics<sup>56-60</sup>. However, previous work on  
493 interbacterial competition has shown that fast growth protects recipient cells from T6SS by establishing stable  
494 microcolonies more quickly than T6SS can kill the recipient cell type<sup>61,62</sup>. Our study suggests that slow recipient  
495 growth could also offer a fitness advantage against lytic T6SS effectors. Similarly to how dead (unlysed) cells can  
496 physically block T6SS-wielding competitors from progressing in space<sup>63</sup>, slow-growing cells could also absorb  
497 T6SS attacks to protect their kin in community settings. A compelling direction for future work could be to  
498 determine if slowing cell growth by an orthogonal mechanism, such as a bonafide stringent response, is sufficient  
499 to recapitulate resistance to Tae1 or other lytic T6SS effectors.

500  
501 A surprising feature of lysis resistance in *msbA-KD* was its tolerance to PG damage by Tae1 alongside additional  
502 damage to its IM and OM. Structural destabilization of the cell envelope commonly renders *Eco* hypersensitive to  
503 lysis<sup>64,65</sup>. However, our observations suggest that integrity of individual envelope components is not always  
504 sufficient to explain cell lysis. Indeed, PG and the OM can work together to bear cellular turgor pressure changes  
505 by sharing the mechanical load across both surfaces<sup>66</sup>. The damaged OM observed in *msbA-KD* could therefore  
506 maintain its turgor-bearing properties to protect cells against lysis when Tae1 hydrolyzes PG. Additionally, the  
507 mechanical integrity of the cell envelope in *msbA-KD* may be fortified by covalently-bound Braun's lipoprotein or  
508 changes to membrane composition which could increase cell envelope stiffness<sup>67,68</sup>. Another unique feature for  
509 *msbA-KD* is that its LPS damage does not stimulate PG remodeling, unlike other depletion alleles for  
510 LPS biosynthesis affecting transport to the OM<sup>31</sup>. We suggest that this indicates multiple nodes for co-regulation  
511 between PG synthesis and LPS synthesis pathways with distinct phenotypic consequences. In line with this  
512 hypothesis, our screen revealed opposing Tae1 sensitivity phenotypes for KDs of *lptC* (LPS transport to OM;  
513 sensitive) and every other LPS hit from the screen (Lipid A-Kdo<sub>2</sub> synthesis/transport; resistant). This observation  
514 invites deeper investigation into the potential for multiple types of LPS and PG crosstalk which may inform the  
515 complex underpinnings of mechanical integrity within the bacterial cell envelope.

516  
517 Another key insight from our study is that PG synthesis is stimulated in response to Tae1, indicative of an active  
518 *Eco* counterresponse. However, wild-type levels of PG synthesis were coincident with, not counter to, lytic death.  
519 Diminished PG synthesis activity in *msbA-KD* could therefore enable resistance by suppressing a toxic  
520 dysregulation of homeostatic activities. We propose that Tae1 activity leads to *Eco* cell death, in part, by triggering  
521 a futile cycle of Tae1 hydrolysis and PG synthesis that does not resolve in cell wall homeostasis. An exciting  
522 prospect for future studies could involve determining the molecular mechanisms that control PG synthesis  
523 stimulation after Tae1 hydrolysis, including whether Tae1 may also synergize or hijack specific endogenous cell  
524 wall enzymes to amplify its damage to PG<sup>69</sup>. The dynamic regulation of PG features indirect to Tae1's peptide  
525 target, such as the glycan backbone, interpeptide crosslinks (type and amount), and recycling could also intersect  
526 with the toxin's acute function to affect its overall impact on the cell wall.

527  
528 In conclusion, our work highlights how recipient susceptibility in interbacterial competition may be more complex  
529 than direct -substrate interactions alone. Toxins with essential targets not only impact specific molecules but also  
530 a dynamic network of interconnected pathways. T6SSs often encode multiple toxins that antagonize different

531 essential features<sup>70</sup>, including components of the cell envelope and other metabolic pathways. We posit that  
532 T6SSs deploy a cocktail of toxins that can act in coordination to disrupt the network beyond repair, or even  
533 weaponize protective homeostatic mechanisms themselves. This study points to the importance of studying the  
534 role of essential genes in the context of T6SS-mediated bacterial antagonism.

## 535 METHODS

536

537

### Bacterial growth and selection

538 *Escherichia coli* strains were cultured in LB or LB-no salt (LBNS) at 37°C with orbital shaking. *Pseudomonas*  
539 *aeruginosa* strains were cultured in LB+ 0.01% Triton at 37°C with orbital shaking. Interbacterial competitions  
540 between *Eco* and *Pae*, and all *Eco* assays requiring solid growth, were conducted on LB+agar or LBNS+agar  
541 plates at 30°C. Where necessary, bacterial strains and plasmids were selected for growth using the following  
542 antibiotics: carbenicillin (Carb; 50 µg/ml) (Grainger), chloramphenicol (Chl; 25 µg/ml) (MP Biomedicals),  
543 gentamicin (Gent; 50 µg/ml)(Alfa Aesar), irgasan (Irg; 25 µg/ml) (Sigma-Aldrich), trimethoprim (Trm;15 µg/ml)  
544 (Sigma-Aldrich), or kanamycin (Kan; 50 µg/ml.) (VWR).

545

546

### Eco CRISPRi library construction and use

547 The *Eco* CRISPRi collection was received in pooled format as a gift from the laboratory of Carol Gross (UCSF).  
548 CRISPRi strains were derived from K12 strain BW25113<sup>71</sup> and are each engineered with a chromosomal insertion  
549 of *dcas9* (constitutive expression) and a custom sgRNA sequence for inducible dCas9-mediated knockdown of a  
550 single gene-of-interest<sup>35</sup>. Transcriptional knockdown is induced with addition of 100µM IPTG (“induced”) into  
551 growth media, though growth without inductant also results in a mild knockdown phenotype (“basal”)<sup>35</sup>. Except  
552 where indicated, CRISPRi knockdown is induced in this study. CRISPRi strains *msbA-KD* and *lpxK-KD* were  
553 reconstructed from the parent strain for individual use in this study. Reconstructed strains were validated by  
554 Sanger sequencing (of the sgRNA and dCas9 chromosomal inserts), qRT-PCR (for knockdown efficiency), and  
555 Western blot (for dCas9 expression). See **Table S1** for strain descriptions and **Table S2** for primer sequences  
556 used for construction and validation.

557

558

### Pae strain construction

559 *Pae* <sup>$\Delta$ tae1</sup> ( $\Delta$ retS $\Delta$ pppA $\Delta$ tae1; *clpV-GFP*) and *Pae*<sup>inactive</sup> ( $\Delta$ retS $\Delta$ pppA $\Delta$ icmF; *clpV-GFP*) strains were constructed  
560 from biparental mating of parent strain *Pae*<sup>WT</sup> (B515: PAO1  $\Delta$ retS $\Delta$ pppA; *clpV-GFP*)<sup>72</sup> with *Eco* SM10  $\lambda$ pir<sup>73</sup>  
561 bearing suicide vector pEXG2 cloned with homology to the gene(s) of interest and a spacer sequence for  
562 replacement. pEXG2 plasmids were cloned using splice-overlap extension<sup>11</sup>. After mating, transformants were  
563 isolated by negative selection on LB-agar + 5% sucrose and confirmed as scarless knockout mutants by colony  
564 PCR of the locus of interest. See **Table S1** for strain descriptions and **Table S2** for primer sequences used for  
565 construction and validation.

566

567

### Pooled interbacterial competition screen

568 Competition assays were performed with overnight *Pae* cultures (*Pae*<sup>WT</sup>, *Pae* <sup>$\Delta$ tae1</sup>, *Pae*<sup>inactive</sup>) and pooled *Eco*  
569 CRISPRi libraries. Flash-frozen glycerol stocks of *Eco* pools were resuspended in LB, backdiluted to OD<sub>600</sub>=0.25,  
570 and recovered for 90 minutes at 37°C with shaking. All cultures were washed twice with fresh LB, then OD<sub>600</sub>-  
571 adjusted to 2.0 (for *Pae*) or 1.0 (for *Eco*) in either LB (basal CRISPRi) or LB+100µM IPTG (induced CRISPRi) . An  
572 aliquot of each CRISPRi pool was reserved by pelleting and flash-freezing for sequencing-based analysis of strain  
573 abundances in the starting population. Media-matched *Pae* and *Eco* were mixed at a 1:1 volumetric ratio, except  
574 for *Eco*<sup>ctrl</sup> populations (for which *Eco* pools were not mixed with *Pae*). Six, 10µl aliquots of coculture were applied  
575 to nitrocellulose membranes (0.2µm, GVS) atop LB-agar (basal CRISPRi) or LB-agar +100µM IPTG (induced  
576 CRISPRi) plates to match liquid media conditions. Covering the agar surface with nitrocellulose allows for nutrient  
577 transfer from the media to the bacteria, while aiding in bacterial recovery from the surface after competition.  
578 Cocultures were dried down to the membrane under flame-sterilization, then incubated at 30°C for 6h. Cocultures  
579 were removed from the plate by scalpel-excision of surrounding nitrocellulose and resuspended into 1ml fresh  
580 PBS by bead-beating for 45s on a tabletop vortex. The six aliquots per experiment were pooled, centrifuged (2min  
581 at 9000xG, RT), and PBS was decanted. Pellets were flash frozen in liquid nitrogen and stored at -80°C.

582

583

### Sequencing library preparation

584 Genomic DNA was extracted from frozen bacterial pellets by phenol: chloroform extraction and RNase  
585 treatment<sup>74</sup>, followed by quantification on a Nanodrop 2000 spectrophotometer (Thermo Scientific). PCR  
586 amplification was used to isolate *Eco* sgRNA sequences from mixed genomic DNA and to attach Illumina Truseq  
587 index adapters for high-throughput sequencing. Sequencing libraries were purified by gel electrophoresis on 8%  
588 TBE gels (Invitrogen Novex), stained with SYBR Gold (Invitrogen) to visualize library bands, and scalpel-excised  
589 (200-300bp region) under blue light imaging (Azure Biosystems c600). Excised libraries were gel-extracted and  
590 precipitated<sup>75</sup>, then resuspended in nuclease-free distilled water (Invitrogen UltraPure). Library concentration was  
591 quantified on a Qubit 2.0 fluorimeter (Invitrogen) using the dsDNA high-sensitivity assay, and assayed for purity  
592 on a 2100 Bioanalyzer (Agilent) using the high-sensitivity DNA assay. Single-end sequencing was performed on  
593 an Illumina NextSeq 500 using a custom sequencing primer and a read length of 75bp. Multiplexed samples were



594 spiked with 5% PhiX Control v3 DNA (Illumina) to account for low diversity among sgRNA sequences. See **Table**  
595 **S2** for custom primers used for library preparation and sequencing.

### 596 **Sequencing data analysis**

597 Raw FASTQ files were aligned to the library oligos and counted using ScreenProcessing  
598 (<https://github.com/mhorlbeck/ScreenProcessing>). Counts were normalized to a total of 20,000,000 reads,  
599 pseudocounts of 1 were added, and  $\log_2$  fold change (L2FC) from t0 was calculated for each strain with at least  
600 100 counts at t0. L2FC was further corrected by subtracting the median L2FC of the non-targeting control  
601 sgRNAs from that sample<sup>76</sup>. The L2FC of each sgRNA were averaged across four biological replicates to  
602 calculate the L2FC for that condition. Finally, to account for differences in the number of generations experienced  
603 (growth) in each of the experimental conditions, L2FC values for the *Pae*<sup>WT</sup>, *Pae* <sup>$\Delta$ tae1</sup>, *Pae*<sup>inactive</sup> experiments were  
604 corrected by the coefficient of a robust (MM-type) intercept free linear regression between the experimental L2FC  
605 values and the CRISPRi induction-matched (induced/basal) *Eco*<sup>ctrl</sup> experiment. See Table S3 for correction  
606 coefficients and corrected L2FC values. Differences between conditions were then calculated for each sgRNA as:

$$607 \text{Diff} = (\text{L2FC} [\textit{condition}]) - (\text{L2FC} \textit{Eco}^{\textit{ctrl}})$$

608  
609 Final Diff values are listed in **Table S4** and were used for all further analyses.

### 610 **COG analysis**

611 Gene ontology information was compiled from the NIH Database of Clusters of Orthologous Genes (COGs)  
612 (<https://www.ncbi.nlm.nih.gov/research/cog>) and reported previously<sup>35</sup>.

### 613 **Data availability and software**

614 Illumina sequencing data from this study is accessible at the NCBI Sequence Read Archive under accession  
615 PRJNA917770. Principal component analysis was performed using R<sup>77</sup> and visualized using ggplot2<sup>78</sup>. All other  
616 data visualizations were prepared using GraphPad Prism 9.4.1 (GraphPad Software, San Diego, California USA,  
617 [www.graphpad.com](http://www.graphpad.com)).

### 618 **Pairwise Interbacterial T6SS competition assay**

619 Competition assays were performed with overnight liquid cultures of *Pae* and *Eco* CRISPRi strains. *Eco* cultures  
620 were backdiluted 1:4 in LB-no salt (LBNS; cite) + 100 $\mu$ M IPTG and grown for 1h at 37°C with shaking to pre-  
621 induce CRISPRi before competition. Strains were washed and mixed in a 1:1 volumetric ratio of *Pae* (OD<sub>600</sub>=2)  
622 and *Eco* (OD<sub>600</sub>=1) in LBNS+100 $\mu$ M IPTG. Three, 10 $\mu$ l aliquots of each liquid co-culture applied to nitrocellulose  
623 membranes (0.2 $\mu$ m, GVS) atop LB-agar+100 $\mu$ M IPTG and dried down by flame-sterilization to encourage  
624 interbacterial competition. Cocultures were incubated at 30°C for 6h. For initial *Eco* colony-forming unit  
625 measurements (CFU<sub>t=0h</sub>), 20 $\mu$ l of each liquid co-culture input was serially diluted (10-fold dilutions x 8) in a 96-well  
626 plate (Corning) and plated onto LB-agar + Gent (*Eco*-selective). After the competition, coculture spots were  
627 harvested from the plate by scalpel-excision of the surrounding nitrocellulose, and pooled by resuspension into  
628 1ml fresh PBS by bead-beating for 45s on a tabletop vortex. Resuspensions were serially diluted (10x8) and  
629 plated onto LB+Gent. All serial dilution plates were incubated overnight at 37°C. Dilution plates with  
630 approximately 20-200 colonies-per-plate were counted for *Eco* CFU abundance (CFU<sub>t=0h</sub>, CFU<sub>t=6h</sub>). Fold-change  
631 in *Eco* CFUs was determined by back-calculating CFUs per ml from dilution plates, and then calculating  
632 CFU<sub>t=6h</sub>/CFU<sub>t=0h</sub>. Experiment was performed for three biological replicates. Statistical test: two-tailed unpaired t-  
633 test.

### 634 **qRT-PCR**

635 Overnight cultures of *Eco* were washed and OD<sub>600</sub>-corrected to 1.0 in LB or LBNS +/-100 $\mu$ l IPTG. Three, 10 $\mu$ l  
636 aliquots of each culture were applied to nitrocellulose membranes (0.2 $\mu$ m, GVS) atop LB-agar+100 $\mu$ M IPTG or  
637 LBNS-agar+100 $\mu$ M IPTG and dried down by flame-sterilization. After growing 6 hours at 30°C, the spots were  
638 scalpel-excised, pooled, and resuspended into PBS by bead beating, then pelleted for RNA extraction. RNA was  
639 extracted using TRIzol Reagent (Invitrogen) with Max Bacterial Enhancement Reagent (Invitrogen), followed by  
640 treatment with Turbo DNA-free kit (Invitrogen) to remove contaminating DNA. After quantification by Nanodrop  
641 (Thermo Scientific), total RNA was reverse transcribed into cDNA using qScript cDNA Supermix (QuantaBio). A  
642 1:5 dilution of cDNA and custom primers were input into qPCR reactions with PowerUP SYBR Green Master Mix  
643 (Applied Biosystems).qRT-PCR was performed using a QuantStudio 3 Real Time PCR system (ThermoFisher  
644 Scientific) using cycling parameters as defined by the master mix instructions. Fold-change in transcript levels  
645 was calculated using  $\Delta\Delta C_t$  analysis, using *rpoD* as a control gene. Three biological and three technical replicates  
646

652 were used per experiment. Statistical test: two-tailed unpaired t-test. Custom primers for qPCR of *Eco* genes can  
653 be found in Table 3.

654

### 655 **Cryo-ET imaging**

656 Overnight cultures of *E. coli* strains were diluted in LB 1:100 and grown at 37°C. At OD<sub>600</sub>=0.2, 150 μM IPTG was  
657 added to the liquid culture to induce CRISPRi knockdown. Bacteria were grown for another 90 min and then flash-  
658 frozen in liquid nitrogen. Cell cultures were mixed with 10 nm protein A gold at 20:1 ratio (Utrecht), then aliquots  
659 of 3 μL mixtures were applied to glow-discharged R2/2, 200 mesh copper Quantifoil grids (Quantifoil Micro Tools).  
660 The sample was blotted for 3 s at 20°C and at 80% humidity. The grids were plunge-frozen in liquid ethane using  
661 Leica EM GP system (Leica Microsystems) and stored in liquid nitrogen. Cryo-ET was performed on a Talos  
662 electron microscope equipped with a Ceta CCD camera (ThermoFisher). Images were taken at magnification  
663 22,000x corresponding to a pixel size of 6.7 Å. Tilt series were collected using SerialEM<sup>79</sup> with a continuous tilt  
664 scheme (-48° to 48°, every 3° increment). The defocus was set to -6 to -8 μm and the cumulative exposure per tilt  
665 series was 150 e<sup>-</sup>/Å<sup>2</sup>. Tomograms were reconstructed with the IMOD software package<sup>80</sup>.

666

### 667 **Overexpression plasmid construction and use**

668 Plasmids for periplasmic Tae1 overexpression in *Eco* were constructed using splice-overlap extension cloning of  
669 *tae1*<sup>WT</sup> and *tae1*<sup>C30A</sup> coding sequences derived from *P. aeruginosa* (PAO1) into *pBAD24*<sup>48,81</sup>. A *pelB* leader  
670 sequence was fused to *tae1* for localization to the periplasm. Expression from *pBAD24* plasmids transformed into  
671 *Eco* was induced by addition of 0.125% arabinose (w/v) (Spectrum Chemical) into liquid LBNS media at early log  
672 phase (OD<sub>600</sub> ~0.25). Overexpression constructs for *msbA* and *lpxK* were constructed by cloning each full-length  
673 gene from *Eco* into the NdeI/HindIII restriction sites of *pSCRhaB2*<sup>82</sup>. Overexpression from *pSCRhaB2* plasmids  
674 transformed into *Eco* was induced by addition of 0.1% rhamnose (w/v) (Thermo Scientific) into liquid media. See  
675 **Table S2** for primer sequences used for cloning and PCR validation.

676

### 677 **Tae1 overexpression lysis assay**

678 Chemically competent *Eco* were transformed with Tae1 overexpression constructs (*pBAD24::tae1*<sup>WT</sup>,  
679 *pBAD24::tae1*<sup>C30A</sup>, *pBAD24*) by standard 42°C heat-shock and a 45-minute recovery in LB at 37°C with shaking.  
680 A transformant population was selected overnight in liquid LB+Carb; the more-traditional method of selecting on  
681 solid media was skipped to discourage the formation of Tae1-resistant compensatory mutations. Overnight  
682 transformant cultures were backdiluted to OD<sub>600</sub>=0.1 in LBNS+Carb +/- 100μM IPTG, then incubated in a Synergy  
683 H1 plate reader (BioTek) at 37°C with shaking (2 technical x 3 biological replicates). OD<sub>600</sub> reads were taken  
684 every five minutes to generate a growth curve. At OD<sub>600</sub>=0.25 (early log-phase), Tae1 expression was induced  
685 from *pBAD24* with the addition of 0.125% arabinose to each well, and grown for 500 minutes at 37°C with  
686 shaking. Bacterial growth curves were normalized to blank growth curves (LBNS+Carb, no bacteria), and average  
687 growth curves from all biological and technical replicates were plotted in Prism (GraphPad).

688

689 For *msbA* and *lpxK* complementation assays, *pSCRhaB2* plasmids were transformed alongside *pBAD24* plasmids,  
690 and overnight selection was performed in liquid LB+Carb+Trm. The next day, cultures were washed and  
691 backdiluted at OD<sub>600</sub>=0.1 into LBNS+Carb+Trm+0.1% rhamnose. The experiment then proceeded in the plate  
692 reader as described above.

693

### 694 **Western blotting**

695 *dCas9 detection*: Total protein was extracted from the organic layer of bacterial pellets treated with TRIzol  
696 Reagent (prepared as described in **qRT-PCR**), according to manufacturer's protocol. Protein samples were  
697 diluted to 1mg/ml in PBS + 1x Laemmli denaturing buffer, boiled for 10 minutes then centrifuged at 20,000xg at  
698 RT for 2 minutes. Fifteen μl of supernatant was loaded onto an anyKD MiniPROTEAN gel (BioRad), alongside  
699 ProteinPlus Ladder (BioRad). Gels were run according to manufacturer's protocol in 1x SDS-PAGE running buffer  
700 to separate proteins. Protein was transferred to nitrocellulose (0.2μm; GVS) via semi-dry transfer with a TransBlot  
701 Turbo transfer system (BioRad) and matching transfer buffer (BioRad) under the following conditions: 45 min @  
702 15V, 2.5 Amp. Transfer was validated by Ponceau stain. Blots were blocked for one hour at RT with shaking in  
703 3% milk+TBST. Primary antibody was applied: 1:1000 mouse anti-Cas9 (Abcam ab191468) in TBST, overnight,  
704 at 4C with shaking. Blots were washed four times in TBST. Secondary antibody was applied: 1:5000 anti-mouse  
705 HRP (Avansta R-05071-500) in TBST, for one hour at RT, with shaking. Blots were washed four times in TBST.  
706 Blots were treated with Clarity ECL Western blotting substrate (BioRad) for chemiluminescent detection on an  
707 Azure c400 imager. Visible light images were also taken to visualize protein ladder. Densitometry analysis was  
708 performed in Fiji<sup>83,84</sup>. Statistical test: two-tailed unpaired t-test. Three biological replicates.

709 *Tae1 detection*: Chemically competent *Eco* cells were transformed with Tae1 overexpression constructs  
710 (*pBAD24::tae1*<sup>WT</sup>, *pBAD24::tae1*<sup>C30A</sup>, *pBAD24*) by standard 42°C heat-shock and a 45-minute recovery in LB at

711 37°C with shaking. A transformant population was selected overnight in liquid LB+Carb. Cultures were  
712 backdiluted to OD<sub>600</sub>=0.1 in LBNS + Carb +100µM IPTG, then incubated in a Synergy H1 plate reader (BioTek) at  
713 37°C with shaking (2 technical x 3 biological replicates). OD<sub>600</sub> reads were taken every five minutes to track  
714 population growth. At OD<sub>600</sub>=0.25, Tae1 expression was induced with the addition of 0.125% arabinose to each  
715 well. Bacteria were grown for 60 minutes with Tae1 induction, before technical replicates were harvested and  
716 pooled. Samples were pelleted by centrifugation and media was decanted before cells were resuspended in PBS  
717 + 1x Laemmli denaturing buffer. Western blotting protocol then proceeded as above, excepting the use of a  
718 custom rabbit anti-Tae1 primary antibody (1:2500 in TBST) (ThermoFisher) and anti-rabbit HRP secondary  
719 antibody (1:5000 in TBST) (Advansta R-05072-500).

720

### 721 Muropeptide analysis

722 Chemically competent *Eco* cells were transformed with Tae1 overexpression constructs (*pBAD24::tae1<sup>WT</sup>*,  
723 *pBAD24::tae1<sup>C30A</sup>*, *pBAD24*) by standard 42°C heat-shock and a 45-minute recovery in LB at 37°C with shaking.  
724 A transformant population was selected overnight in liquid LB+Carb. Cultures were backdiluted to OD<sub>600</sub>=0.1 in  
725 LBNS+Carb +100µM IPTG, and grown with shaking. At early log phase (OD<sub>600</sub>=0.25), 0.125% arabinose was  
726 added to induce *pBAD24* expression. Cells were grown for 60 minutes, then harvested by centrifugation. For PG  
727 purification, cells were boiled in 3% SDS to extract crude PG, then treated with Pronase E (100µg/ml in Tris-HCl  
728 (pH 7.2) + 0.06% NaCl) (VWR Chemicals) for 2 hours at 60C to remove proteins covalently bound to PG.  
729 Mutanolysin digestion (40µg/ml in Tris-HCl (pH 7.2) + 0.06% NaCl) was performed overnight at 37C to solubilize  
730 PG into muropeptides for HPLC analysis. Samples were reduced with sodium borohydride (Fisher Chemical) then  
731 pH-corrected to 3-4 using o-phosphoric acid(Fisher Chemical)<sup>85</sup>. Muropeptides were separated on a 1220 Infinity  
732 II HPLC (Agilent) with UV-visible detection (λ=206nm). Muropeptide separation was achieved over 54 minutes at  
733 0.5 ml/min using a Hypersil ODS C18 column (Thermo Scientific) and a gradient elution from 50mM sodium  
734 phosphate + 0.04% NaN<sub>3</sub> (Buffer A) to 75mM sodium phosphate +15% methanol (Buffer B). Chromatograms  
735 were integrated in ChemStation software (Agilent) to determine peak area, height, and elution time. Experimental  
736 chromatograms were normalized against a chromatogram from a blank run (ddH<sub>2</sub>O). Chromatograms were also  
737 internally normalized against the most abundant M4 (monomer muropeptide) peak; this allowed for direct relative  
738 comparisons of peak heights between samples.

739

740 To calculate the percent change in D44 (4,3-crosslinked dimer) peptides after Tae1 overexpression, the  
741 normalized area under the curve (AUC) for D44 was divided by the total chromatogram area to calculate the  
742 relative D44 peak area for each condition (AUC<sub>WT</sub>, AUC<sub>C30A</sub>, AUC<sub>EV</sub>). Then, within a given strain,  
743 (AUC<sub>WT</sub>/AUC<sub>EV</sub>)\*100 and (AUC<sub>C30A</sub>/AUC<sub>EV</sub>)\*100 were calculated to determine the percent of D44 peak area lost to  
744 Tae1<sup>WT</sup> or Tae1<sup>C30A</sup> treatment, relative to EV treatment. Three biological replicates were performed per condition.  
745 Statistical test: two-tailed unpaired t-test.

746

### 747 HADA incorporation imaging

748 Chemically competent cells were transformed with *pBAD24* constructs: (*pBAD24::tae1<sup>WT</sup>*, *pBAD24::tae1<sup>C30A</sup>*, or  
749 *pBAD24*) and selected with Carb overnight in liquid LB. Transformant cultures were backdiluted to OD<sub>600</sub>=0.1 in  
750 1ml LBNS+Carb +100µM IPTG, and grown with shaking. At early log phase (OD<sub>600</sub>=0.25), 0.125% arabinose  
751 added to induce *pBAD24* expression. Cells were grown for 30 minutes, then 250µM HADA added to culture. Cells  
752 were grown an additional 30 minutes, then collected by centrifugation and washed 3x with cold PBS + sodium  
753 citrate (pH 3.0) to block hydrolysis of labelled septal PG<sup>86</sup>. Cells were fixed by treatment with 3% PFA for 15  
754 minutes on ice. Fixed cells were washed 3x in cold PBS, then resuspended in PBS +20% DMSO. Fluorescence  
755 imaging was performed on a Nikon Eclipse Ti2-E inverted microscope equipped with a 100x/1.40 oil-immersion  
756 phase objective and an EMCCD camera (Prime 95B). Fluorescence (DAPI channel) and phase-contrast images  
757 were captured using NIS-Elements AR Viewer 5.20. Images were analyzed for single-cell fluorescence intensity  
758 using MicrobeJ for Fiji<sup>84,87</sup>. 200 cells/sample measured, 3 biological replicates. Statistical test: unpaired t-test.

759

### 760 Nascent protein synthesis imaging

761 Chemically competent cells were transformed with *pBAD24* constructs: (*pBAD24::tae1<sup>WT</sup>*, *pBAD24::tae1<sup>C30A</sup>*, or  
762 *pBAD24*) and selected with Carb overnight in liquid LB. Cultures were diluted by 1:100 and grown in LBNS+ Carb+  
763 100µM IPTG at 37 °C with shaking. At early log phase (~80 minutes) 0.125% arabinose was added to induce Tae1  
764 expression. After 35 minutes, 13µM O-propargyl-puromycin (OPP) was added to cultures to label new peptide  
765 synthesis before harvesting (Click-iT™ Plus OPP Alexa Fluor™ 488 Protein Synthesis Assay Kit, Invitrogen)<sup>88</sup>. After  
766 labelling, cells were pelleted and fixed in 3.7% formaldehyde in PBS. Cells were permeabilized with 0.3% Triton X-  
767 100 in PBS for 15 min, then labelled for imaging with Click-iT reaction cocktail for 20 min in the dark, washed then  
768 resuspended in PBS. Fluorescence imaging was performed on a Nikon Eclipse Ti2-E inverted microscope equipped  
769 with a 100x/1.40 oil-immersion objective and an EMCCD camera (Prime 95B). The 488-nm laser illumination



770 fluorescence and phase-contrast images were captured using NIS-Elements AR Viewer 5.20 and analyzed using  
771 MicrobeJ software for Fiji<sup>84,87</sup>.

772

### 773 **Time-lapse imaging of T6SS competitions**

774 Competition microscopy experiments were performed with overnight liquid cultures of *Pae* (LB) and *Eco* CRISPRi  
775 strains (LB+Gent+Cam). Cultures were diluted 1:50 in fresh medium and grown for 2h. *Pae* cells were diluted  
776 again 1:50 in fresh medium (LB) and grown at 37°C to OD 1.2 – 1.5 (~1 hour). Similarly, *E. coli* strains were  
777 diluted 1:100 in fresh medium (LB+150µM IPTG) supplemented with antibiotics (Gent / Cam) and grown at 37°C  
778 to OD 1.2 – 1.5 (~1 hour). Then, cultures were washed with LB, resuspended in LB + 150µM IPTG and mixed 2:1  
779 (*Pae:Eco*). 1 µl of the mixed cells was spotted on an agarose pad containing propidium iodide and imaged for 2h  
780 at 37°C. A Nikon Ti-E inverted motorized microscope with Perfect Focus System and Plan Apo 1003 Oil Ph3 DM  
781 (NA 1.4) objective lens was used to acquire images. If not indicated otherwise, time-lapse series of competitions  
782 were acquired at 10 s acquisition frame rate during 120 min. SPECTRA X light engine (Lumencore), ET-GFP  
783 (Chroma #49002) and ET-mCherry (Chroma #49008) filter sets were used to excite and filter fluorescence.  
784 VisiView software (Visitron Systems, Germany) was used to record images with a sCMOS camera pco.edge 4.2  
785 (PCO, Germany) (pixel size 65 nm). The power output of the SPECTRA X light engine was set to 20% for all  
786 excitation wavelengths. GFP, phase-contrast and RFP / propidium iodide (PI) images were acquired with 50-100  
787 ms exposure time. Temperature and humidity were set to 37°C, 95% respectively, using an Okolab T-unit  
788 objective heating collar as well as a climate chamber (Okolab). Fiji was used for imaging processing<sup>84</sup>. Acquired  
789 time-lapse series were drift-corrected using a custom StackReg based software<sup>89,90</sup>.

790

### 791 **SUPPLEMENTAL INFORMATION**

792 **Table S1.** Bacterial strains and plasmids used in this study

793 **Table S2.** Primer sequences

794 **Table S3.** Corrected L2FC values from screen

795 **Table S4.** Final Diff values from screen

796

### 797 **ACKNOWLEDGEMENTS**

798

799 We are grateful to all members of the Chou and Basler labs for their support throughout this project (with special  
800 thanks to Atanas Radkov, Krisna Van Dyke, Sebastian Flores, and Eleanor Wang). We thank Carol Gross  
801 (UCSF) and members of her lab (Jason Peters, Marco Jost, John Hawkins) for their assistance in adapting their  
802 CRISPRi system for our project. We thank Michelle Tan, Rene Sit, and Norma Neff (Chan-Zuckerberg Biohub) for  
803 assistance with high-throughput sequencing. We thank Naomi Ziv (UCSF), and DeLaine Larsen and Kari  
804 Harrington (UCSF Nikon Imaging Center) for assistance with fluorescence microscopy. We are grateful to KC  
805 Huang (Stanford University), Waldemar Vollmer (Newcastle University), and Alessandra Polissi (University of  
806 Milan) for fruitful conversations regarding the complex biology of the bacterial cell envelope. We thank Sandra  
807 Catania and Lauren Trotta for their generous feedback toward data analysis and manuscript preparation.

808

809 This work was funded by: NIH NIAID award T32AI060535 (KLT), a UCSF Moritz-Heyman Discovery Fellowship  
810 (KLT), the Swiss National Science Foundation (grant BSSGI0\_155778) (MB), a European Research Council  
811 consolidator grant (865105 -"AimingT6SS") (MB), the Chan-Zuckerberg Biohub (SC), and the Pew Biomedical  
812 Scholars Program (SC).

813

### 814 **AUTHOR CONTRIBUTIONS**

815 Kristine L Trotta (Conceptualization, Methodology, Research, Data analysis, Data visualization, Writing,  
816 Reviewing)

817 Beth M Hayes (Conceptualization, Research, Data analysis, Reviewing)

818 Johannes P Schneider (Methodology, Research, Data analysis, Reviewing)

819 Jing Wang (Methodology, Research, Data analysis, Reviewing)

820 Horia Todor (Data analysis, Data visualization, Reviewing)

821 Patrick Rockefeller Grimes (Research, Reviewing)

822 Ziyi Zhao (Methodology, Research, Data analysis, Reviewing)

823 William L Hatleberg (Data visualization, Reviewing)

824 Melanie R Silvis (Conceptualization, Methodology, Reviewing)

825 Rachel Kim (Methodology, Reviewing)

826 Byoung-Mo Koo (Methodology, Reviewing)

827 Marek Basler (Project administration, Reviewing)

828 Seemay Chou (Project administration, Funding, Conceptualization, Writing, Reviewing)



829

830

**COMPETING INTERESTS**

831

The authors declare no competing interests. Seemay Chou is the president and CEO of Arcadia Science.

832  
833  
834  
835  
836  
837  
838  
839  
840  
841  
842  
843  
844  
845  
846  
847  
848  
849  
850  
851  
852  
853  
854  
855  
856  
857  
858  
859  
860  
861  
862  
863  
864  
865  
866  
867  
868  
869  
870  
871  
872  
873  
874  
875  
876  
877  
878  
879  
880  
881  
882  
883  
884  
885  
886  
887  
888  
889  
890

## REFERENCES

- (1) Ghoul, M.; Mitri, S. The Ecology and Evolution of Microbial Competition. *Trends Microbiol* **2016**, *24* (10), 833–845. <https://doi.org/10.1016/j.tim.2016.06.011>.
- (2) Granato, E. T.; Meiller-Legrand, T. A.; Foster, K. R. The Evolution and Ecology of Bacterial Warfare. *Current Biology* **2019**, *29* (11), R521–R537. <https://doi.org/10.1016/j.cub.2019.04.024>.
- (3) Boyer, F.; Fichant, G.; Berthod, J.; Vandenbrouck, Y.; Attree, I. Dissecting the Bacterial Type VI Secretion System by a Genome Wide in Silico Analysis: What Can Be Learned from Available Microbial Genomic Resources? *BMC Genomics* **2009**, *10*, 104. <https://doi.org/10.1186/1471-2164-10-104>.
- (4) Basler, M. Type VI Secretion System: Secretion by a Contractile Nanomachine. *Philos Trans R Soc Lond B Biol Sci* **2015**, *370* (1679), 20150021. <https://doi.org/10.1098/rstb.2015.0021>.
- (5) Pukatzki, S.; Ma, A. T.; Sturtevant, D.; Krastins, B.; Sarracino, D.; Nelson, W. C.; Heidelberg, J. F.; Mekalanos, J. J. Identification of a Conserved Bacterial Protein Secretion System in *Vibrio Cholerae* Using the Dictyostelium Host Model System. *Proc Natl Acad Sci U S A* **2006**, *103* (5), 1528–1533. <https://doi.org/10.1073/pnas.0510322103>.
- (6) Hood, R. D.; Singh, P.; Hsu, F.; Güvener, T.; Carl, M. A.; Trinidad, R. R. S.; Silverman, J. M.; Ohlson, B. B.; Hicks, K. G.; Plemel, R. L.; Li, M.; Schwarz, S.; Wang, W. Y.; Merz, A. J.; Goodlett, D. R.; Mougous, J. D. A Type VI Secretion System of *Pseudomonas Aeruginosa* Targets a Toxin to Bacteria. *Cell Host Microbe* **2010**, *7* (1), 25–37. <https://doi.org/10.1016/j.chom.2009.12.007>.
- (7) Mougous, J. D.; Cuff, M. E.; Raunser, S.; Shen, A.; Zhou, M.; Gifford, C. A.; Goodman, A. L.; Joachimiak, G.; Ordoñez, C. L.; Lory, S.; Walz, T.; Joachimiak, A.; Mekalanos, J. J. A Virulence Locus of *Pseudomonas Aeruginosa* Encodes a Protein Secretion Apparatus. *Science* **2006**, *312* (5779), 1526–1530. <https://doi.org/10.1126/science.1128393>.
- (8) Chou, S.; Bui, N. K.; Russell, A. B.; Lexa, K. W.; Gardiner, T. E.; LeRoux, M.; Vollmer, W.; Mougous, J. D. Structure of a Peptidoglycan Amidase Effector Targeted to Gram-Negative Bacteria by the Type VI Secretion System. *Cell Reports* **2012**, *1* (6), 656–664. <https://doi.org/10.1016/j.celrep.2012.05.016>.
- (9) Ho, B. T.; Basler, M.; Mekalanos, J. J. Type 6 Secretion System-Mediated Immunity to Type 4 Secretion System-Mediated Horizontal Gene Transfer. *Science* **2013**, *342* (6155), 250–253. <https://doi.org/10.1126/science.1243745>.
- (10) LeRoux, M.; Kirkpatrick, R. L.; Montauti, E. I.; Tran, B. Q.; Peterson, S. B.; Harding, B. N.; Whitney, J. C.; Russell, A. B.; Traxler, B.; Goo, Y. A.; Goodlett, D. R.; Wiggins, P. A.; Mougous, J. D. Kin Cell Lysis Is a Danger Signal That Activates Antibacterial Pathways of *Pseudomonas Aeruginosa*. *eLife* **4**. <https://doi.org/10.7554/eLife.05701>.
- (11) Russell, A. B.; Hood, R. D.; Bui, N. K.; LeRoux, M.; Vollmer, W.; Mougous, J. D. Type VI Secretion Delivers Bacteriolytic Effectors to Target Cells. *Nature* **2011**, *475* (7356), 343–347. <https://doi.org/10.1038/nature10244>.
- (12) Whitney, J. C.; Chou, S.; Russell, A. B.; Biboy, J.; Gardiner, T. E.; Ferrin, M. A.; Brittnacher, M.; Vollmer, W.; Mougous, J. D. Identification, Structure, and Function of a Novel Type VI Secretion Peptidoglycan Glycoside Hydrolase Effector-Immunity Pair \*. *Journal of Biological Chemistry* **2013**, *288* (37), 26616–26624. <https://doi.org/10.1074/jbc.M113.488320>.
- (13) Whitney, J. C.; Quentin, D.; Sawai, S.; LeRoux, M.; Harding, B. N.; Ledvina, H. E.; Tran, B. Q.; Robinson, H.; Goo, Y. A.; Goodlett, D. R.; Raunser, S.; Mougous, J. D. An Interbacterial NAD(P)<sup>+</sup> Glycohydrolase Toxin Requires Elongation Factor Tu for Delivery to Target Cells. *Cell* **2015**, *163* (3), 607–619. <https://doi.org/10.1016/j.cell.2015.09.027>.
- (14) LaCourse, K. D.; Peterson, S. B.; Kulasekara, H. D.; Radey, M. C.; Kim, J.; Mougous, J. D. Conditional Toxicity and Synergy Drive Diversity among Antibacterial Effectors. *Nat Microbiol* **2018**, *3* (4), 440–446. <https://doi.org/10.1038/s41564-018-0113-y>.
- (15) Pissaridou, P.; Allsopp, L. P.; Wettstadt, S.; Howard, S. A.; Mavridou, D. A. I.; Filloux, A. The *Pseudomonas Aeruginosa* T6SS-VgrG1b Spike Is Topped by a PAAR Protein Eliciting DNA Damage to Bacterial Competitors. *Proc Natl Acad Sci U S A* **2018**, *115* (49), 12519–12524. <https://doi.org/10.1073/pnas.1814181115>.
- (16) Höltje, J.-V. Growth of the Stress-Bearing and Shape-Maintaining Murein Sacculus of *Escherichia Coli*. *Microbiol Mol Biol Rev* **1998**, *62* (1), 181–203.
- (17) Pazos, M.; Peters, K. Peptidoglycan. In *Bacterial Cell Walls and Membranes*; Kuhn, A., Ed.; Subcellular Biochemistry; Springer International Publishing: Cham, 2019; pp 127–168. [https://doi.org/10.1007/978-3-030-18768-2\\_5](https://doi.org/10.1007/978-3-030-18768-2_5).
- (18) Russell, A. B.; Singh, P.; Brittnacher, M.; Bui, N. K.; Hood, R. D.; Carl, M. A.; Agnello, D. M.; Schwarz, S.; Goodlett, D. R.; Vollmer, W.; Mougous, J. D. A Widespread Bacterial Type VI Secretion Effector Superfamily Identified Using a Heuristic Approach. *Cell Host & Microbe* **2012**, *11* (5), 538–549. <https://doi.org/10.1016/j.chom.2012.04.007>.

- 891 (19) Shang, G.; Liu, X.; Lu, D.; Zhang, J.; Li, N.; Zhu, C.; Liu, S.; Yu, Q.; Zhao, Y.; Zhang, H.; Hu, J.; Cang, H.; Xu,  
892 S.; Gu, L. Structural Insight into How *Pseudomonas Aeruginosa* Peptidoglycanhydrolase Tse1 and Its  
893 Immunity Protein Tsi1 Function. *Biochemical Journal* **2012**, *448* (2), 201–211.  
894 <https://doi.org/10.1042/BJ20120668>.
- 895 (20) Ding, J.; Wang, W.; Feng, H.; Zhang, Y.; Wang, D.-C. Structural Insights into the *Pseudomonas Aeruginosa*  
896 Type VI Virulence Effector Tse1 Bacteriolysis and Self-Protection Mechanisms. *J Biol Chem* **2012**, *287* (32),  
897 26911–26920. <https://doi.org/10.1074/jbc.M112.368043>.
- 898 (21) Hersch, S. J.; Watanabe, N.; Stietz, M. S.; Manera, K.; Kamal, F.; Burkinshaw, B.; Lam, L.; Pun, A.; Li, M.;  
899 Savchenko, A.; Dong, T. G. Envelope Stress Responses Defend against Type Six Secretion System Attacks  
900 Independently of Immunity Proteins. *Nat Microbiol* **2020**, *5* (5), 706–714. [https://doi.org/10.1038/s41564-](https://doi.org/10.1038/s41564-020-0672-6)  
901 [020-0672-6](https://doi.org/10.1038/s41564-020-0672-6).
- 902 (22) Kamal, F.; Liang, X.; Manera, K.; Pei, T.-T.; Kim, H.; Lam, L. G.; Pun, A.; Hersch, S. J.; Dong, T. G.  
903 Differential Cellular Response to Translocated Toxic Effectors and Physical Penetration by the Type VI  
904 Secretion System. *Cell Reports* **2020**, *31* (11), 107766. <https://doi.org/10.1016/j.celrep.2020.107766>.
- 905 (23) Toska, J.; Ho, B. T.; Mekalanos, J. J. Exopolysaccharide Protects *Vibrio Cholerae* from Exogenous Attacks  
906 by the Type 6 Secretion System. *Proceedings of the National Academy of Sciences* **2018**, *115* (31), 7997–  
907 8002. <https://doi.org/10.1073/pnas.1808469115>.
- 908 (24) Pérez-Lorente, A. I.; Molina-Santiago, C.; de Vicente, A.; Romero, D. *Sporulation Activated via  $\sigma^W$  Protects*  
909 *Bacillus from a Tse1 Peptidoglycan Hydrolase T6SS Effector*; preprint; Microbiology, 2022.  
910 <https://doi.org/10.1101/2022.02.23.481616>.
- 911 (25) Dong, T. G.; Dong, S.; Catalano, C.; Moore, R.; Liang, X.; Mekalanos, J. J. Generation of Reactive Oxygen  
912 Species by Lethal Attacks from Competing Microbes. *Proc Natl Acad Sci U S A* **2015**, *112* (7), 2181–2186.  
913 <https://doi.org/10.1073/pnas.1425007112>.
- 914 (26) Crisan, C. V.; Nichols, H. L.; Wiesenfeld, S.; Steinbach, G.; Yunker, P. J.; Hammer, B. K. Glucose Confers  
915 Protection to *Escherichia Coli* against Contact Killing by *Vibrio Cholerae*. *Sci Rep* **2021**, *11*, 2935.  
916 <https://doi.org/10.1038/s41598-021-81813-4>.
- 917 (27) Typas, A.; Banzhaf, M.; Gross, C. A.; Vollmer, W. From the Regulation of Peptidoglycan Synthesis to  
918 Bacterial Growth and Morphology. *Nat Rev Microbiol* **2011**, *10* (2), 123–136.  
919 <https://doi.org/10.1038/nrmicro2677>.
- 920 (28) Yang, D. C.; Tan, K.; Joachimiak, A.; Bernhardt, T. G. A Conformational Switch Controls Cell Wall-  
921 Remodelling Enzymes Required for Bacterial Cell Division. *Mol Microbiol* **2012**, *85* (4), 768–781.  
922 <https://doi.org/10.1111/j.1365-2958.2012.08138.x>.
- 923 (29) Delhaye, A.; Collet, J.-F.; Laloux, G. Fine-Tuning of the Cpx Envelope Stress Response Is Required for Cell  
924 Wall Homeostasis in *Escherichia Coli*. *mBio* **2016**, *7* (1), e00047-16. <https://doi.org/10.1128/mBio.00047-16>.
- 925 (30) Peters, K.; Kannan, S.; Rao, V. A.; Biboy, J.; Vollmer, D.; Erickson, S. W.; Lewis, R. J.; Young, K. D.; Vollmer,  
926 W. The Redundancy of Peptidoglycan Carboxypeptidases Ensures Robust Cell Shape Maintenance in  
927 *Escherichia Coli*. *mBio* **2016**, *7* (3), e00819-16. <https://doi.org/10.1128/mBio.00819-16>.
- 928 (31) Morè, N.; Martorana, A. M.; Biboy, J.; Otten, C.; Winkle, M.; Serrano, C. K. G.; Montón Silva, A.; Atkinson, L.;  
929 Yau, H.; Breukink, E.; den Blaauwen, T.; Vollmer, W.; Polissi, A. Peptidoglycan Remodeling Enables  
930 *Escherichia Coli* To Survive Severe Outer Membrane Assembly Defect. *mBio* **2019**, *10* (1), e02729-18.  
931 <https://doi.org/10.1128/mBio.02729-18>.
- 932 (32) Mueller, E. A.; Egan, A. J.; Breukink, E.; Vollmer, W.; Levin, P. A. Plasticity of *Escherichia Coli* Cell Wall  
933 Metabolism Promotes Fitness and Antibiotic Resistance across Environmental Conditions. *Elife* **2019**, *8*,  
934 e40754. <https://doi.org/10.7554/eLife.40754>.
- 935 (33) Lin, H.-H.; Yu, M.; Sriramoju, M. K.; Hsu, S.-T. D.; Liu, C.-T.; Lai, E.-M. A High-Throughput Interbacterial  
936 Competition Screen Identifies ClpAP in Enhancing Recipient Susceptibility to Type VI Secretion System-  
937 Mediated Attack by *Agrobacterium Tumefaciens*. *Front Microbiol* **2020**, *10*, 3077.  
938 <https://doi.org/10.3389/fmicb.2019.03077>.
- 939 (34) Hersch, S. J.; Sejuty, R. T.; Manera, K.; Dong, T. G. *High Throughput Identification of Genes Conferring*  
940 *Resistance or Sensitivity to Toxic Effectors Delivered by the Type VI Secretion System*; preprint;  
941 Microbiology, 2021. <https://doi.org/10.1101/2021.10.06.463450>.
- 942 (35) Silvis, M. R.; Rajendram, M.; Shi, H.; Osadnik, H.; Gray, A. N.; Cesar, S.; Peters, J. M.; Hearne, C. C.;  
943 Kumar, P.; Todor, H.; Huang, K. C.; Gross, C. A. Morphological and Transcriptional Responses to CRISPRi  
944 Knockdown of Essential Genes in *Escherichia Coli*. *mBio* **2021**, *12* (5), e02561-21.  
945 <https://doi.org/10.1128/mBio.02561-21>.
- 946 (36) Kampmann, M.; Bassik, M. C.; Weissman, J. S. Integrated Platform for Genome-Wide Screening and  
947 Construction of High-Density Genetic Interaction Maps in Mammalian Cells. *PNAS* **2013**, *110* (25), E2317–  
948 E2326. <https://doi.org/10.1073/pnas.1307002110>.

- 949 (37) Horlbeck, M. A.; Gilbert, L. A.; Villalta, J. E.; Adamson, B.; Pak, R. A.; Chen, Y.; Fields, A. P.; Park, C. Y.;  
950 Corn, J. E.; Kampmann, M.; Weissman, J. S. Compact and Highly Active Next-Generation Libraries for  
951 CRISPR-Mediated Gene Repression and Activation. *Elife* **2016**, 5. <https://doi.org/10.7554/eLife.19760>.
- 952 (38) Silhavy, T. J.; Kahne, D.; Walker, S. The Bacterial Cell Envelope. *Cold Spring Harb Perspect Biol* **2010**, 2 (5),  
953 a000414. <https://doi.org/10.1101/cshperspect.a000414>.
- 954 (39) Klein, G.; Raina, S. Regulated Control of the Assembly and Diversity of LPS by Noncoding SRNAs. *Biomed*  
955 *Res Int* **2015**, 2015. <https://doi.org/10.1155/2015/153561>.
- 956 (40) Bertani, B.; Ruiz, N. Function and Biogenesis of Lipopolysaccharides. *EcoSal Plus* **2018**, 8 (1).  
957 <https://doi.org/10.1128/ecosalplus.ESP-0001-2018>.
- 958 (41) Klein, G.; Raina, S. Regulated Assembly of LPS, Its Structural Alterations and Cellular Response to LPS  
959 Defects. *Int J Mol Sci* **2019**, 20 (2), 356. <https://doi.org/10.3390/ijms20020356>.
- 960 (42) Guest, R. L.; Rutherford, S. T.; Silhavy, T. J. Border Control: Regulating LPS Biogenesis. *Trends in*  
961 *Microbiology* **2021**, 29 (4), 334–345. <https://doi.org/10.1016/j.tim.2020.09.008>.
- 962 (43) Garrett, T. A.; Kadmas, J. L.; Raetz, C. R. Identification of the Gene Encoding the Escherichia Coli Lipid A 4'-  
963 Kinase. *J Biol Chem* **1997**, 272 (35), 21855–21864. <https://doi.org/10.1074/jbc.272.35.21855>.
- 964 (44) Garrett, T. A.; Que, N. L. S.; Raetz, C. R. H. Accumulation of a Lipid A Precursor Lacking the 4'-Phosphate  
965 Following Inactivation of the Escherichia Coli LpxK Gene \*. *Journal of Biological Chemistry* **1998**, 273 (20),  
966 12457–12465. <https://doi.org/10.1074/jbc.273.20.12457>.
- 967 (45) Karow, M.; Georgopoulos, C. The Essential Escherichia Coli MsbA Gene, a Multicopy Suppressor of Null  
968 Mutations in the HtrB Gene, Is Related to the Universally Conserved Family of ATP-Dependent  
969 Translocators. *Mol Microbiol* **1993**, 7 (1), 69–79. <https://doi.org/10.1111/j.1365-2958.1993.tb01098.x>.
- 970 (46) Polissi, A.; Georgopoulos, C. Mutational Analysis and Properties of the MsbA Gene of Escherichia Coli,  
971 Coding for an Essential ABC Family Transporter. *Molecular Microbiology* **1996**, 20 (6), 1221–1233.  
972 <https://doi.org/10.1111/j.1365-2958.1996.tb02642.x>.
- 973 (47) Alexander, M. K.; Miu, A.; Oh, A.; Reichelt, M.; Ho, H.; Chalouni, C.; Labadie, S.; Wang, L.; Liang, J.;  
974 Nickerson, N. N.; Hu, H.; Yu, L.; Du, M.; Yan, D.; Park, S.; Kim, J.; Xu, M.; Sellers, B. D.; Purkey, H. E.;  
975 Skelton, N. J.; Koehler, M. F. T.; Payandeh, J.; Verma, V.; Xu, Y.; Koth, C. M.; Nishiyama, M. Disrupting  
976 Gram-Negative Bacterial Outer Membrane Biosynthesis through Inhibition of the Lipopolysaccharide  
977 Transporter MsbA. *Antimicrob Agents Chemother* **2018**, 62 (11), e01142-18.  
978 <https://doi.org/10.1128/AAC.01142-18>.
- 979 (48) Radkov, A.; Sapiro, A. L.; Flores, S.; Henderson, C.; Saunders, H.; Kim, R.; Massa, S.; Thompson, S.;  
980 Mateusiak, C.; Biboy, J.; Zhao, Z.; Starita, L. M.; Hatleberg, W. L.; Vollmer, W.; Russell, A. B.; Simorre, J.-  
981 P.; Anthony-Cahill, S.; Brzovic, P.; Hayes, B.; Chou, S. Antibacterial Potency of Type VI Amidase Effector  
982 Toxins Is Dependent on Substrate Topology and Cellular Context. *eLife* **2022**, 11, e79796.  
983 <https://doi.org/10.7554/eLife.79796>.
- 984 (49) Desmarais, S. M.; De Pedro, M. A.; Cava, F.; Huang, K. C. Peptidoglycan at Its Peaks: How  
985 Chromatographic Analyses Can Reveal Bacterial Cell Wall Structure and Assembly. *Molecular Microbiology*  
986 **2013**, 89 (1), 1–13. <https://doi.org/10.1111/mmi.12266>.
- 987 (50) Egan, A. J. F.; Errington, J.; Vollmer, W. Regulation of Peptidoglycan Synthesis and Remodelling. *Nat Rev*  
988 *Microbiol* **2020**, 18 (8), 446–460. <https://doi.org/10.1038/s41579-020-0366-3>.
- 989 (51) Egan, A. J. F.; Cleverley, R. M.; Peters, K.; Lewis, R. J.; Vollmer, W. Regulation of Bacterial Cell Wall Growth.  
990 *FEBS J* **2017**, 284 (6), 851–867. <https://doi.org/10.1111/febs.13959>.
- 991 (52) Scherrer, R.; Moyed, H. S. Conditional Impairment of Cell Division and Altered Lethality in HipA Mutants of  
992 Escherichia Coli K-12. *J Bacteriol* **1988**, 170 (8), 3321–3326.
- 993 (53) Kwan, B. W.; Valenta, J. A.; Benedik, M. J.; Wood, T. K. Arrested Protein Synthesis Increases Persister-Like  
994 Cell Formation. *Antimicrob Agents Chemother* **2013**, 57 (3), 1468–1473. <https://doi.org/10.1128/AAC.02135-12>.
- 995 (54) Liu, S.; Wu, N.; Zhang, S.; Yuan, Y.; Zhang, W.; Zhang, Y. Variable Persister Gene Interactions with  
996 (p)PpGpp for Persister Formation in Escherichia Coli. *Frontiers in Microbiology* **2017**, 8.
- 997 (55) Roghianian, M.; Semsey, S.; Løbner-Olesen, A.; Jalalvand, F. (P)PpGpp-Mediated Stress Response Induced  
998 by Defects in Outer Membrane Biogenesis and ATP Production Promotes Survival in Escherichia Coli. *Sci*  
999 *Rep* **2019**, 9 (1), 2934. <https://doi.org/10.1038/s41598-019-39371-3>.
- 1000 (56) Łoś, M.; Golec, P.; Łoś, J. M.; Węglewska-Jurkiewicz, A.; Czyż, A.; Węgrzyn, A.; Węgrzyn, G.; Neubauer, P.  
1001 Effective Inhibition of Lytic Development of Bacteriophages λ, P1 and T4 by Starvation of Their Host,  
1002 Escherichia Coli. *BMC Biotechnology* **2007**, 7 (1), 13. <https://doi.org/10.1186/1472-6750-7-13>.
- 1003 (57) Pearl, S.; Gabay, C.; Kishony, R.; Oppenheim, A.; Balaban, N. Q. Nongenetic Individuality in the Host–Phage  
1004 Interaction. *PLoS Biol* **2008**, 6 (5), e120. <https://doi.org/10.1371/journal.pbio.0060120>.
- 1005

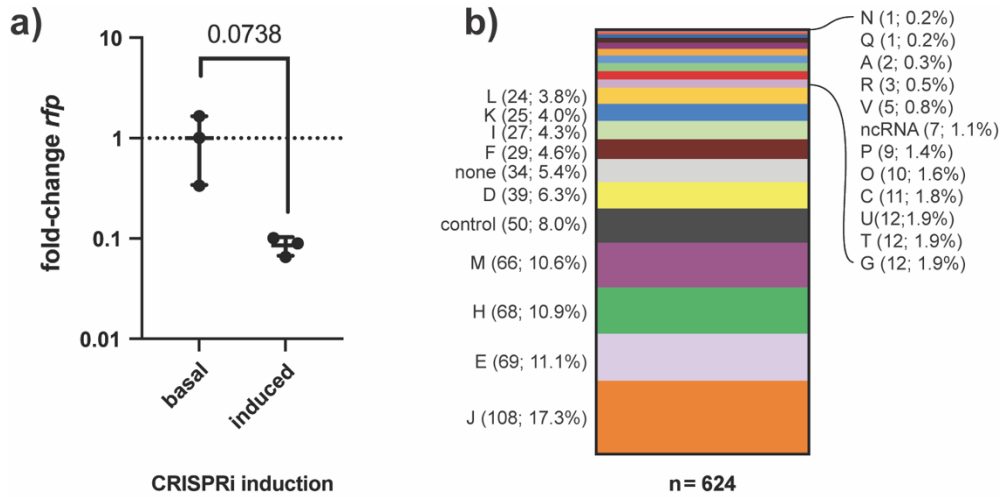


- 1006 (58) Meeske, A. J.; Nakandakari-Higa, S.; Marraffini, L. A. Cas13-Induced Cellular Dormancy Prevents the Rise of  
1007 CRISPR-Resistant Bacteriophage. *Nature* **2019**, *570* (7760), 241–245. <https://doi.org/10.1038/s41586-019->  
1008 1257-5.
- 1009 (59) Wiuff, C.; Zappala, R. M.; Regoes, R. R.; Garner, K. N.; Baquero, F.; Levin, B. R. Phenotypic Tolerance:  
1010 Antibiotic Enrichment of Noninherited Resistance in Bacterial Populations. *Antimicrob Agents Chemother*  
1011 **2005**, *49* (4), 1483–1494. <https://doi.org/10.1128/AAC.49.4.1483-1494.2005>.
- 1012 (60) Lee, A. J.; Wang, S.; Meredith, H. R.; Zhuang, B.; Dai, Z.; You, L. Robust, Linear Correlations between  
1013 Growth Rates and  $\beta$ -Lactam-Mediated Lysis Rates. *Proceedings of the National Academy of Sciences*  
1014 **2018**, *115* (16), 4069–4074. <https://doi.org/10.1073/pnas.1719504115>.
- 1015 (61) Wilmoth, J. L.; Doak, P. W.; Timm, A.; Halsted, M.; Anderson, J. D.; Ginovart, M.; Prats, C.; Portell, X.;  
1016 Retterer, S. T.; Fuentes-Cabrera, M. A Microfluidics and Agent-Based Modeling Framework for Investigating  
1017 Spatial Organization in Bacterial Colonies: The Case of *Pseudomonas Aeruginosa* and H1-Type VI  
1018 Secretion Interactions. *Front Microbiol* **2018**, *9*, 33. <https://doi.org/10.3389/fmicb.2018.00033>.
- 1019 (62) Borenstein, D. B.; Ringel, P.; Basler, M.; Wingreen, N. S. Established Microbial Colonies Can Survive Type VI  
1020 Secretion Assault. *PLOS Computational Biology* **2015**, *11* (10), e1004520.  
1021 <https://doi.org/10.1371/journal.pcbi.1004520>.
- 1022 (63) Smith, W. P. J.; Vettiger, A.; Winter, J.; Ryser, T.; Comstock, L. E.; Basler, M.; Foster, K. R. The Evolution of  
1023 the Type VI Secretion System as a Disintegration Weapon. *PLOS Biology* **2020**, *18* (5), e3000720.  
1024 <https://doi.org/10.1371/journal.pbio.3000720>.
- 1025 (64) Nichols, R. J.; Sen, S.; Choo, Y. J.; Beltrao, P.; Zietek, M.; Chaba, R.; Lee, S.; Kazmierczak, K. M.; Lee, K. J.;  
1026 Wong, A.; Shales, M.; Lovett, S.; Winkler, M. E.; Krogan, N. J.; Typas, A.; Gross, C. A. Phenotypic  
1027 Landscape of a Bacterial Cell. *Cell* **2011**, *144* (1), 143–156. <https://doi.org/10.1016/j.cell.2010.11.052>.
- 1028 (65) Paradis-Bleau, C.; Kritikos, G.; Orlova, K.; Typas, A.; Bernhardt, T. G. A Genome-Wide Screen for Bacterial  
1029 Envelope Biogenesis Mutants Identifies a Novel Factor Involved in Cell Wall Precursor Metabolism. *PLOS*  
1030 *Genetics* **2014**, *10* (1), e1004056. <https://doi.org/10.1371/journal.pgen.1004056>.
- 1031 (66) Rojas, E. R.; Billings, G.; Odermatt, P. D.; Auer, G. K.; Zhu, L.; Miguel, A.; Chang, F.; Weibel, D. B.; Theriot,  
1032 J. A.; Huang, K. C. The Outer Membrane Is an Essential Load-Bearing Element in Gram-Negative Bacteria.  
1033 *Nature* **2018**, *559* (7715), 617–621. <https://doi.org/10.1038/s41586-018-0344-3>.
- 1034 (67) Mathelié-Guinlet, M.; Asmar, A. T.; Collet, J.-F.; Dufrière, Y. F. Lipoprotein Lpp Regulates the Mechanical  
1035 Properties of the *E. Coli* Cell Envelope. *Nat Commun* **2020**, *11*, 1789. <https://doi.org/10.1038/s41467-020->  
1036 15489-1.
- 1037 (68) Effects of Membrane Lipid Composition and Antibacterial Drugs on the Rigidity of *Escherichia Coli*: Different  
1038 Contributions of Various Bacterial Substructures. <https://doi.org/10.1002/sca.21243>.
- 1039 (69) Singh, S. K.; SaiSree, L.; Amrutha, R. N.; Reddy, M. Three Redundant Murein Endopeptidases Catalyse an  
1040 Essential Cleavage Step in Peptidoglycan Synthesis of *Escherichia Coli* K12. *Molecular Microbiology* **2012**,  
1041 *86* (5), 1036–1051. <https://doi.org/10.1111/mmi.12058>.
- 1042 (70) Jurénas, D.; Journet, L. Activity, Delivery, and Diversity of Type VI Secretion Effectors. *Molecular*  
1043 *Microbiology* **2021**, *115* (3), 383–394. <https://doi.org/10.1111/mmi.14648>.
- 1044 (71) Baba, T.; Ara, T.; Hasegawa, M.; Takai, Y.; Okumura, Y.; Baba, M.; Datsenko, K. A.; Tomita, M.; Wanner, B.  
1045 L.; Mori, H. Construction of *Escherichia Coli* K-12 in-Frame, Single-Gene Knockout Mutants: The Keio  
1046 Collection. *Molecular Systems Biology* **2006**, *2* (1), 2006.0008. <https://doi.org/10.1038/msb4100050>.
- 1047 (72) Vettiger, A.; Basler, M. Type VI Secretion System Substrates Are Transferred and Reused among Sister  
1048 Cells. *Cell* **2016**, *167* (1), 99–110.e12. <https://doi.org/10.1016/j.cell.2016.08.023>.
- 1049 (73) Simon, R.; Priefer, U.; Pühler, A. A Broad Host Range Mobilization System for In Vivo Genetic Engineering:  
1050 Transposon Mutagenesis in Gram Negative Bacteria. *Nat Biotechnol* **1983**, *1* (9), 784–791.  
1051 <https://doi.org/10.1038/nbt1183-784>.
- 1052 (74) He, F. E. *Coli* Genomic DNA Extraction. *Bio-101* **2011**, e97. <https://doi.org/10.21769/BioProtoc.97>.
- 1053 (75) Churchman, L. S.; Weissman, J. S. Nascent Transcript Sequencing Visualizes Transcription at Nucleotide  
1054 Resolution. *Nature* **2011**, *469* (7330), 368–373. <https://doi.org/10.1038/nature09652>.
- 1055 (76) Hawkins, J. S.; Silvis, M. R.; Koo, B.-M.; Peters, J. M.; Osadnik, H.; Jost, M.; Hearne, C. C.; Weissman, J. S.;  
1056 Todor, H.; Gross, C. A. Mismatch-CRISPRi Reveals the Co-Varying Expression-Fitness Relationships of  
1057 Essential Genes in *Escherichia Coli* and *Bacillus Subtilis*. *Cell Syst* **2020**, *11* (5), 523–535.e9.  
1058 <https://doi.org/10.1016/j.cels.2020.09.009>.
- 1059 (77) R: A Language and Environment for Statistical Computing. <https://www.R-project.org/>.
- 1060 (78) Wickham, H. *Ggplot2: Elegant Graphics for Data Analysis*; Springer-Verlag New York.
- 1061 (79) Mastronarde, D. N. Automated Electron Microscope Tomography Using Robust Prediction of Specimen  
1062 Movements. *Journal of Structural Biology* **2005**, *152* (1), 36–51. <https://doi.org/10.1016/j.jsb.2005.07.007>.
- 1063 (80) Kremer, J. R.; Mastronarde, D. N.; McIntosh, J. R. Computer Visualization of Three-Dimensional Image Data  
1064 Using IMOD. *J Struct Biol* **1996**, *116* (1), 71–76. <https://doi.org/10.1006/jsbi.1996.0013>.

- 1065 (81) Guzman, L. M.; Belin, D.; Carson, M. J.; Beckwith, J. Tight Regulation, Modulation, and High-Level  
1066 Expression by Vectors Containing the Arabinose PBAD Promoter. *Journal of Bacteriology* **1995**, *177* (14),  
1067 4121–4130. <https://doi.org/10.1128/jb.177.14.4121-4130.1995>.
- 1068 (82) Cardona, S. T.; Valvano, M. A. An Expression Vector Containing a Rhamnose-Inducible Promoter Provides  
1069 Tightly Regulated Gene Expression in Burkholderia Cenocepacia. *Plasmid* **2005**, *54* (3), 219–228.  
1070 <https://doi.org/10.1016/j.plasmid.2005.03.004>.
- 1071 (83) Stael, S.; Miller, L. P.; Fernández-Fernández, Á. D.; Van Breusegem, F. Detection of Damage-Activated  
1072 Metacaspase Activity Activities by Western Blot in Plants. In *Plant Proteases and Plant Cell Death: Methods  
1073 and Protocols*; Klemenčič, M., Stael, S., Huesgen, P. F., Eds.; Methods in Molecular Biology; Springer US:  
1074 New York, NY, 2022; pp 127–137. [https://doi.org/10.1007/978-1-0716-2079-3\\_11](https://doi.org/10.1007/978-1-0716-2079-3_11).
- 1075 (84) Schindelin, J.; Arganda-Carreras, I.; Frise, E.; Kaynig, V.; Longair, M.; Pietzsch, T.; Preibisch, S.; Rueden, C.;  
1076 Saalfeld, S.; Schmid, B.; Tinevez, J.-Y.; White, D. J.; Hartenstein, V.; Eliceiri, K.; Tomancak, P.; Cardona, A.  
1077 Fiji: An Open-Source Platform for Biological-Image Analysis. *Nat Methods* **2012**, *9* (7), 676–682.  
1078 <https://doi.org/10.1038/nmeth.2019>.
- 1079 (85) Desmarais, S. M.; Cava, F.; de Pedro, M. A.; Huang, K. C. Isolation and Preparation of Bacterial Cell Walls  
1080 for Compositional Analysis by Ultra Performance Liquid Chromatography. *J Vis Exp* **2014**, No. 83, 51183.  
1081 <https://doi.org/10.3791/51183>.
- 1082 (86) Peters, K.; Pazos, M.; VanNieuwenhze, M. S.; Vollmer, W. Optimized Protocol for the Incorporation of FDAA  
1083 (HADA Labeling) for in Situ Labeling of Peptidoglycan. *Bio Protoc* **2019**, *9* (15), e3316.  
1084 <https://doi.org/10.21769/BioProtoc.3316>.
- 1085 (87) Ducret, A.; Quardokus, E. M.; Brun, Y. V. MicrobeJ, a Tool for High Throughput Bacterial Cell Detection and  
1086 Quantitative Analysis. *Nat Microbiol* **2016**, *1* (7), 1–7. <https://doi.org/10.1038/nmicrobiol.2016.77>.
- 1087 (88) Diez, S.; Ryu, J.; Caban, K.; Gonzalez, R. L.; Dworkin, J. The Alarmones (p)PpGpp Directly Regulate  
1088 Translation Initiation during Entry into Quiescence. *Proceedings of the National Academy of Sciences* **2020**,  
1089 *117* (27), 15565–15572. <https://doi.org/10.1073/pnas.1920013117>.
- 1090 (89) Ringel, P. D.; Hu, D.; Basler, M. The Role of Type VI Secretion System Effectors in Target Cell Lysis and  
1091 Subsequent Horizontal Gene Transfer. *Cell Rep* **2017**, *21* (13), 3927–3940.  
1092 <https://doi.org/10.1016/j.celrep.2017.12.020>.
- 1093 (90) Thevenaz, P.; Ruttimann, U. E.; Unser, M. A Pyramid Approach to Subpixel Registration Based on Intensity.  
1094 *IEEE Transactions on Image Processing* **1998**, *7* (1), 27–41. <https://doi.org/10.1109/83.650848>.

1095  
1096

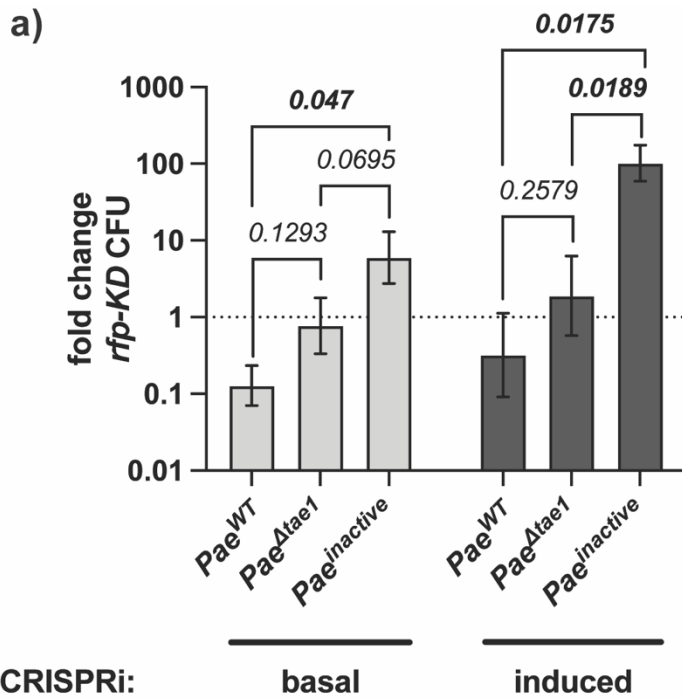
## SUPPLEMENTAL FIGURES



1097  
1098  
1099  
1100  
1101  
1102  
1103  
1104  
1105  
1106

### Supplement 1: CRISPRi conditionally knocks down transcription across hundreds of *Eco* gene targets

**a) CRISPRi induction produces mild transcriptional knockdown of endogenous *rfp* (11.7-fold decrease) in *Eco*.** qRT-PCR measurement of relative *rfp* RNA expression in *Eco* strain SC363 after 6 hours of growth on solid LB media with basal or induced CRISPRi. Data shown: 3 biological replicates with mean  $\pm$  s.d. Statistical test: unpaired two-tailed *t*-test. **b) CRISPRi targets *Eco* genes that collectively represent 21 clusters of orthogonal genes (COGs).** CRISPRi target genes ( $n=596$ ) were binned by their NCBI COG functional assignment. The relative representation of each COG in the strain collection is displayed as a percent of all COGs. Some genes are represented by multiple COGs, resulting in a greater number of COGs ( $n=624$ ) than target genes. Non-targeting negative controls ("control",  $n=50$ ) genes without COG assignments ("none",  $n=34$ ), and genes coding for non-coding RNAs ("ncRNA",  $n=7$ ) were also binned.



1107  
1108  
1109  
1110  
1111  
1112

CRISPRi:

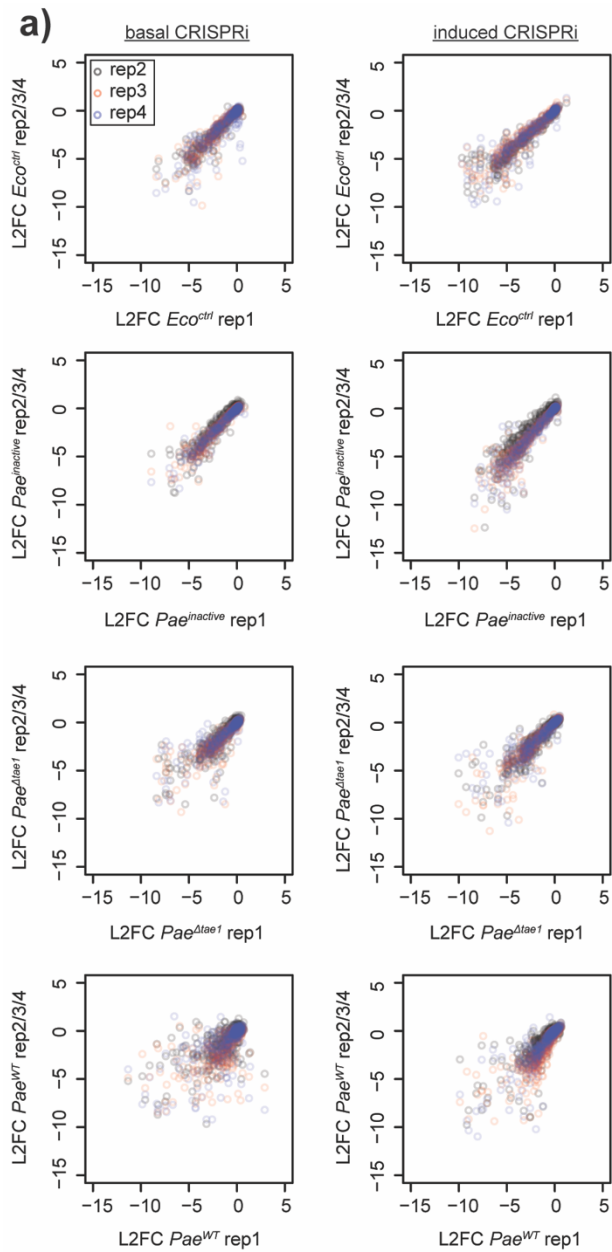
basal

induced

**Supplement 2: Non-targeting CRISPRi induction has little effect on *Eco* fitness in T6SS competition**

a) CRISPRi induction does not disrupt T6SS- and *Tae1*-dependent targeting of *Eco* by *Pae*. Interbacterial competition between *Pae* (*Pae*<sup>WT</sup>, *Pae* <sup>$\Delta$ tae1</sup>, *Pae*<sup>inactive</sup>) and an *Eco* negative-control KD strain (*rfp-KD*), with induced or basal CRISPRi. Data shown: mean fold-change ( $\pm$  geometric s.d.) of *rfp-KD* colony forming units (CFUs) after six hours of competition against *Pae*. Statistical test: unpaired two-tailed *t*-test; *p*-value  $\leq 0.05$  displayed in bold font.

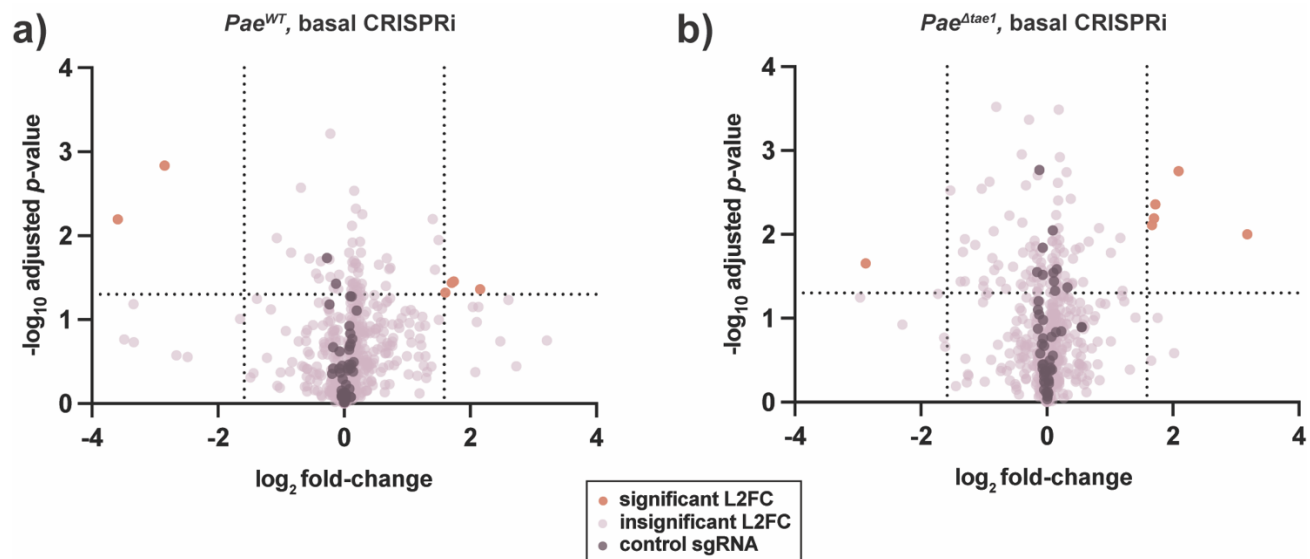




1113  
1114  
1115  
1116  
1117

**Supplement 3: CRISPRi library fitness in T6SS screen is reproducible across biological replicates**

a) **CRISPRi library fitness in T6SS screen is reproducible across biological replicates.** Replica plots showing the uncorrected L2FC values for each *Eco* CRISPRi strain after competition against *Pae*<sup>WT</sup>, *Pae*<sup>Δtae1</sup>, *Pae*<sup>inactive</sup>, for four biological replicates. For each plot, replicate 1 is compared to replicate 2 (grey), replicate 3 (red), or replicate 4 (blue). Median Pearson's *r* between all replicates = 0.91.

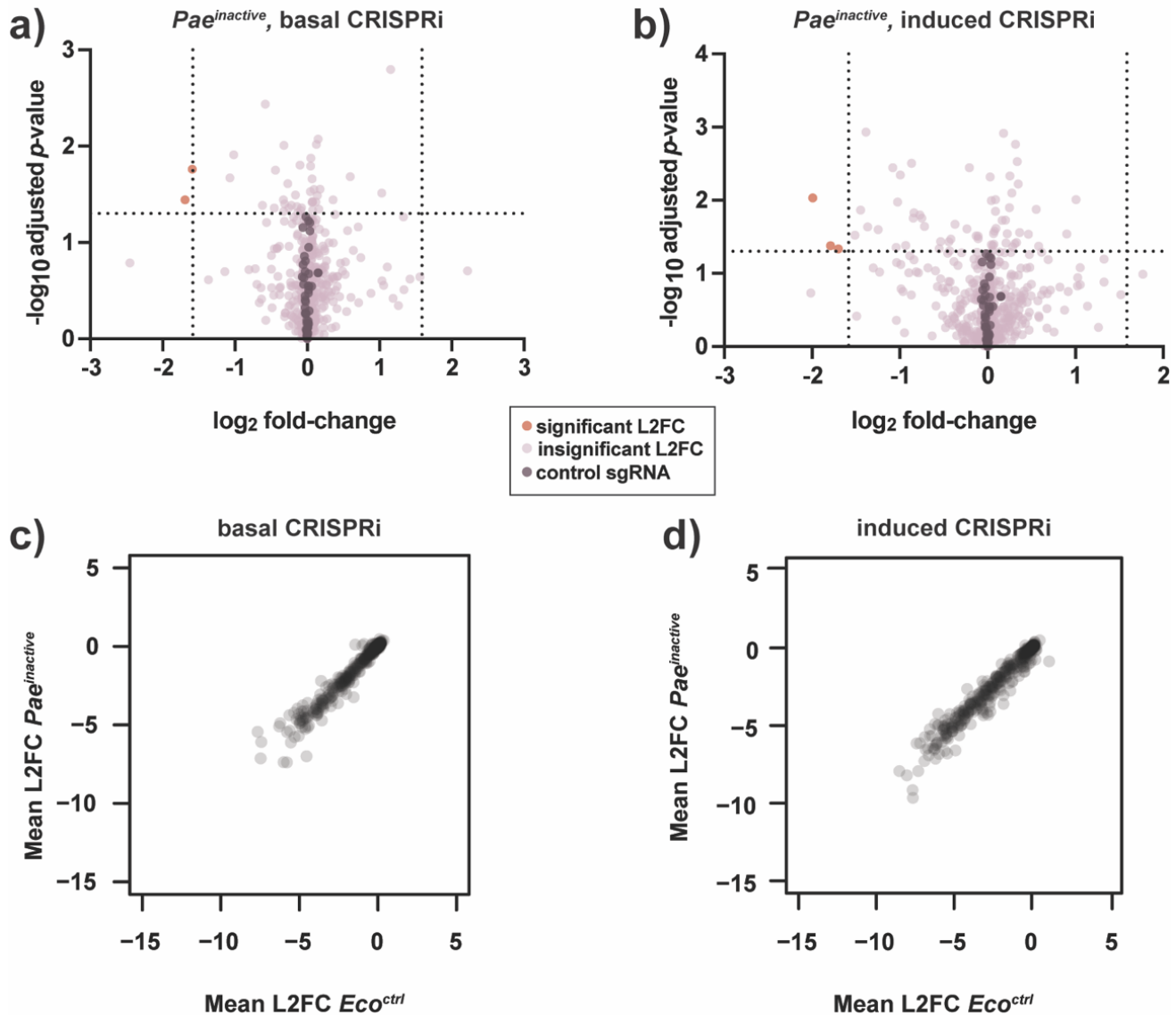


1118  
1119  
1120  
1121  
1122  
1123  
1124  
1125

**Supplement 4: Pooled T6SS competitions with basal CRISPRi attenuate significant fitness phenotypes**

a-b) Basal CRISPRi attenuates *Eco* fitness phenotypes against *Pae<sup>WT</sup>* (a) and *Pae<sup>Δetae1</sup>* (b). Volcano plots showing log<sub>2</sub>-fold change (L2FC) values for each KD strain after interbacterial competition (basal CRISPRi). Data shown: mean from four biological replicates. Statistical test: Wald test. Vertical dotted lines indicate arbitrary cutoffs for L2FC at  $x = -1.58$  and  $x = 1.58$  (absolute FC  $x = -3$  or  $x = 3$ ). Horizontal dotted line indicates statistical significance cutoff for log<sub>10</sub> adjusted  $p$ -value ( $\leq 0.05$ ). Orange points represent KDs with L2FC  $\geq 1.58$  or  $\leq -1.58$  and log<sub>10</sub>-adj.  $p$ -value  $\leq 0.05$ . Dark purple points represent non-targeting negative control KDs ( $n=50$ ). Lavender points represent KDs that do not meet cutoffs for L2FC or statistical test.

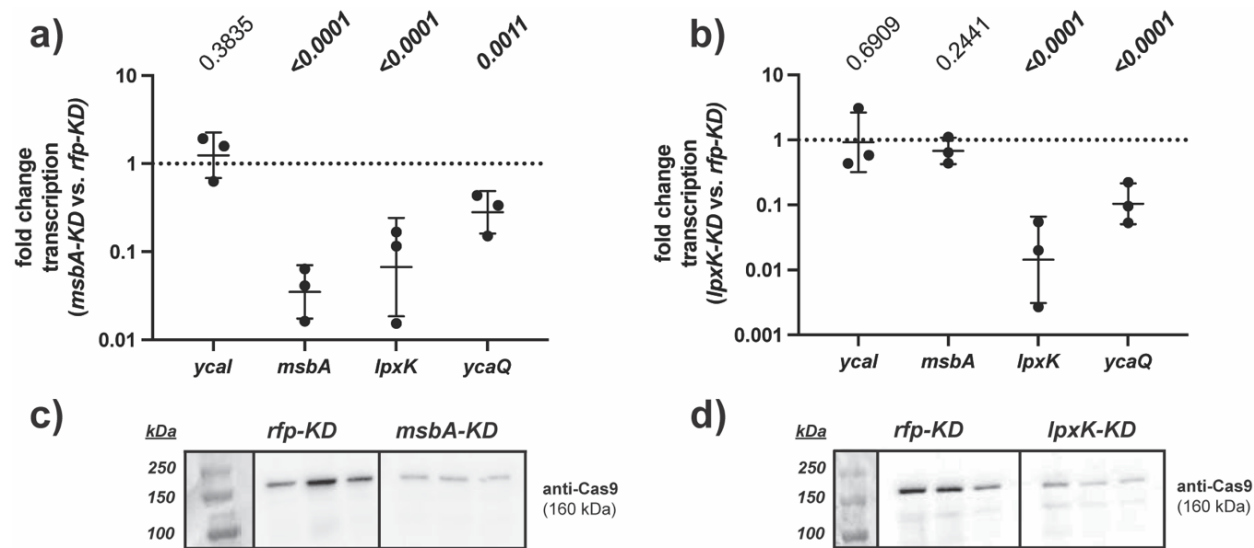
1126



1127  
 1128  
 1129  
 1130  
 1131  
 1132  
 1133  
 1134  
 1135  
 1136

**Supplement 5: *Pae<sup>inactive</sup>* is a neutral co-culture partner for *Eco***

**a-b) Competition against *Pae<sup>inactive</sup>* reveals few *Eco* fitness determinants.** Volcano plots showing log<sub>2</sub>-fold change (L2FC) values for each KD strain after interbacterial competition with induced (a) or basal (b) CRISPRi. Data shown: mean from four biological replicates. Statistical test: Wald test. Vertical dotted lines indicate arbitrary cutoffs for L2FC at x=-1.58 and x=1.58 (absolute FC x=-3 or x=3). Horizontal dotted line indicates statistical significance cutoff for log<sub>10</sub> adjusted p-value (≤ 0.05). Orange points represent KDs with L2FC ≥ 1.58 or ≤ -1.58 and log<sub>10</sub>-adj. p-value ≤ 0.05. Dark purple points represent non-targeting negative control KDs (n=50). Lavender points represent KDs that do not meet cutoffs for L2FC or statistical test. **c-d) KD strain abundance is highly similar after competition with *Pae<sup>inactive</sup>* and after growth without competition (*Eco<sup>ctrl</sup>*).** Scatter plots comparing mean L2FC for each *Eco* KD strain after competition with *Pae<sup>inactive</sup>* or *Eco<sup>ctrl</sup>* treatment, with basal (c) or induced (d) CRISPRi. Median Pearson correlation r = 0.98.

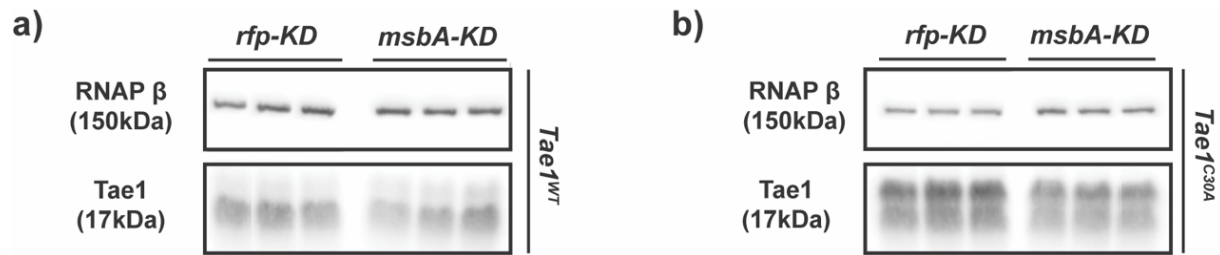


**Supplement 6: *lpxK-KD* and *msbA-KD* modulate target gene expression and show polar effects**

**a-b) Transcriptional knockdowns in *msbA* and *lpxK* have off-target polar effects on transcription in their operon.** qRT-PCR analysis of transcriptional fold-change in *ycaI-msbA-lpxK-ycaQ* in *msbA-KD* (a) and in *lpxK-KD* (b) after growth for 6 hours with induced CRISPRi, normalized to expression in *rfp-KD*. Data shown are geometric average of 3 biological replicates  $\pm$  s.d. Statistical test: unpaired two-tailed *t*-test; *p*-value  $\leq 0.05$  displayed in bold font. **c-d) *msbA-KD* and *lpxK-KD* express a catalytically dead Cas9 (dCas9) enzyme for CRISPRi-mediated transcriptional knockdown.** Western blot analysis of dCas9 protein expression (160 kDa) from *rfp-KD*, *msbA-KD* (c), and *lpxK-KD* (d). Three independent biological replicates shown.

1137  
1138  
1139  
1140  
1141  
1142  
1143  
1144  
1145

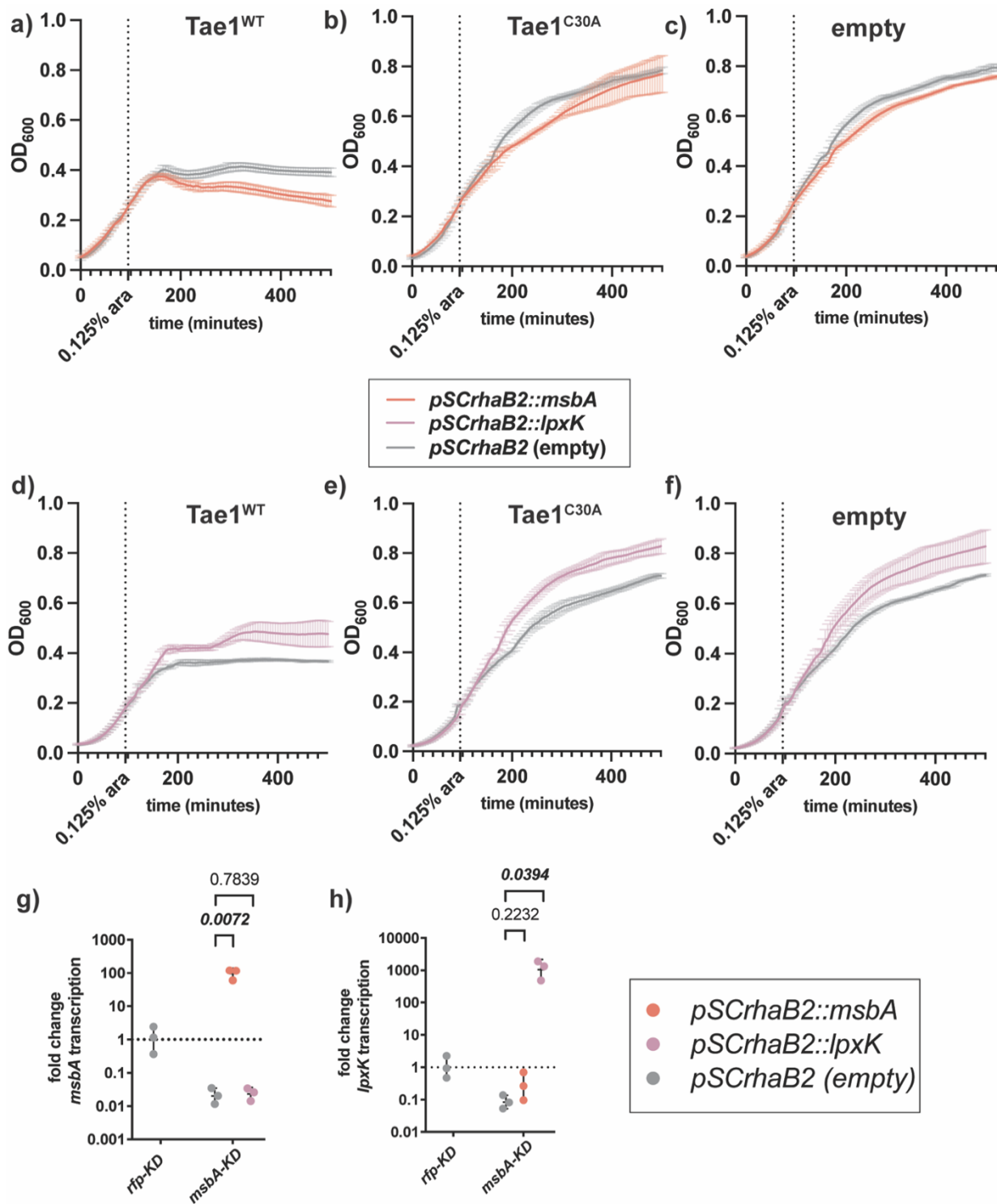




**Supplement 7: Tae1 protein expression is unaffected in *msbA-KD***

**a-b) Bulk Tae1 protein expression is similar between *msbA-KD* and *rfp-KD*.** Western blot analysis of periplasmic Tae1 protein (17kDa) from (a) *pBAD24::pelB-tae1<sup>WT</sup>* (Tae1<sup>WT</sup>) or (b) *pBAD24::pelB-tae1<sup>C30A</sup>* (Tae1<sup>C30A</sup>) in *rfp-KD* and *msbA-KD* (with induced CRISPRi). Protein expression of RNA polymerase (β subunit) (150kDa) is used as an internal loading control.

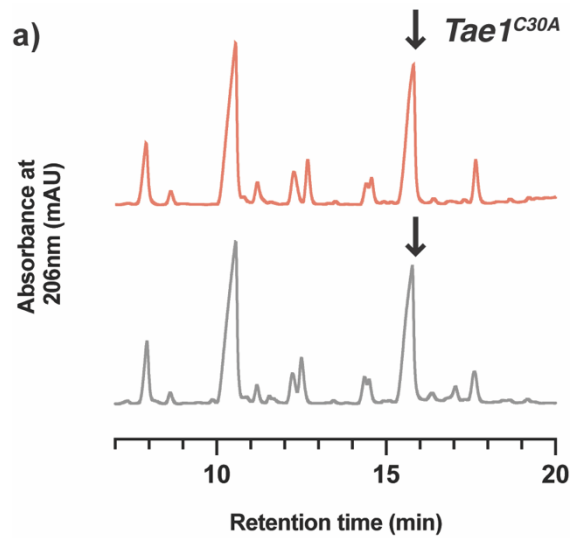
1146  
1147  
1148  
1149  
1150



**Supplement 8: Plasmid-borne overexpression of *msbA* partially rescues *Tae1* sensitivity in *msbA-KD***

a-c) Plasmid-borne *msbA* overexpression partially rescues *msbA-KD* resistance to lysis by *Tae1*. OD<sub>600</sub> growth curves of *msbA-KD* with induced CRISPRi, overexpressing *pSCRhaB2::msbA* (orange) or *pSCRhaB2* (empty) (grey) alongside (a) *pBAD24::pelB-tae1*<sup>WT</sup> (*Tae1*<sup>WT</sup>), (b) *pBAD24::pelB-tae1*<sup>C30A</sup> (*Tae1*<sup>C30A</sup>), or (c) *pBAD24* (empty). Data shown: average of 3 biological replicates ± s.d. Dotted vertical line indicates *pBAD24* induction timepoint (at OD<sub>600</sub>=0.25) (0.125% arabinose w/v). d-f) Plasmid-borne *lpxK* overexpression enhances *msbA-KD* resistance to lysis by *Tae1*. OD<sub>600</sub> growth curves of *msbA-KD* with CRISPRi induced, overexpressing *pSCRhaB2::lpxK* (purple) or *pSCRhaB2* (empty) (grey) alongside (d) *pBAD24::pelB-tae1*<sup>WT</sup> (*Tae1*<sup>WT</sup>), (e) *pBAD24::pelB-tae1*<sup>C30A</sup> (*Tae1*<sup>C30A</sup>), or (f) *pBAD24* (empty). Data shown: average of 3 biological replicates ± s.d. Dotted vertical line indicates *pBAD24* induction timepoint (at OD<sub>600</sub>=0.25) (0.125% arabinose w/v). g-h) *pSCRhaB2* vectors selectively rescue transcription of their target gene by overexpression. qRT-PCR analysis of transcriptional fold-change in (g) *msbA* or (h) *lpxK* expression with constitutive rhamnose induction of *pSCRhaB2::msbA* (orange), *pSCRhaB2::lpxK* (purple), or (c) *pSCRhaB2* (empty; grey) in *msbA-KD* with induced CRISPRi. Expression normalized against basal *msbA* expression in *rfp-KD* + *pSCRhaB2* (empty). Data shown: geometric average of 3 biological replicates ± s.d. Statistical test: unpaired two-tailed t-test; p-value ≤ 0.05 displayed in bold font.

1151  
 1152  
 1153  
 1154  
 1155  
 1156  
 1157  
 1158  
 1159  
 1160  
 1161  
 1162  
 1163  
 1164

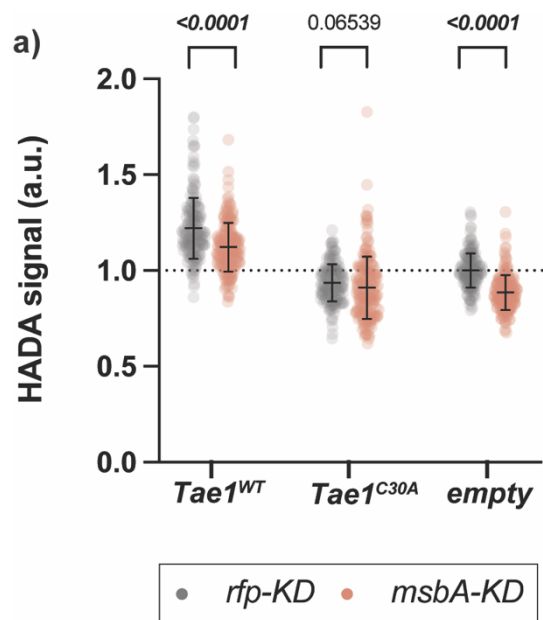


— *msbA-KD* — *rfp-KD*

1165  
1166  
1167  
1168  
1169  
1170

**Supplement 9: *Tae1<sup>C30A</sup>* hydrolyzes D44 muropeptides in *rfp-KD* and *msbA-KD***

a) *Tae1<sup>C30A</sup>* overexpression yields minor digestion of D44 muropeptides. HPLC chromatograms of muropeptides purified from *msbA-KD* (orange) and *rfp-KD* (grey) expressing *pBAD24::peIB-tae1<sup>C30A</sup>* (*Tae1<sup>C30A</sup>*). Black arrow indicates D44 peptide partially digested by *Tae1<sup>C30A</sup>*. Data shown: representative from 3 biological replicates.

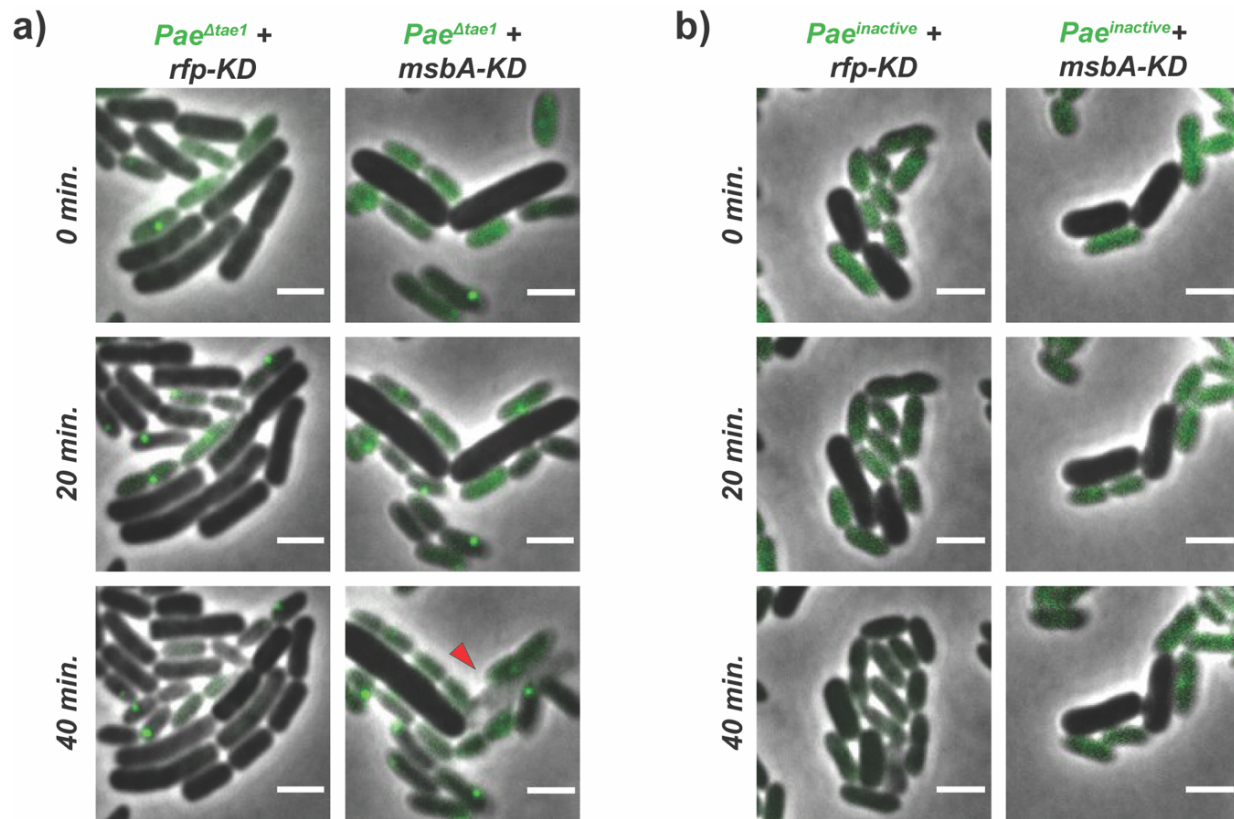


1171  
1172  
1173  
1174  
1175  
1176  
1177

**Supplement 10: PG synthesis activity in *msbA-KD* is suppressed across all conditions**

a) **PG synthesis activity in *msbA-KD* is attenuated under all tested conditions.** Single-cell fluorescence intensity measurements for *rfp-KD* (grey) or *msbA-KD* (orange) incorporating the fluorescent D-amino acid HADA into PG after 60 minutes of overexpressing *pBAD24::peIB-tae1<sup>WT</sup>* ( $Tae1^{WT}$ ), *pBAD24::peIB-tae1<sup>C30A</sup>* ( $Tae1^{C30A}$ ), or *pBAD24* (empty), with CRISPRi induced. All data normalized to average HADA signal in *rfp-KD* + empty. Data shown: 600 cells (200 cells x 3 biological replicates), with average  $\pm$  s.d. Statistical test: unpaired two-tailed *t*-test; *p*-value  $\leq 0.05$  displayed in bold font.





1178  
1179  
1180  
1181  
1182  
1183

**Supplement 11: *msbA-KD* growth defects are independent of *Pae* T6SS activity**

*a-b* *msbA-KD* cells maintain growth defects regardless of *Pae* competitor. Representative frames from time-course imaging of *rfp-KD* (left column; grey cells) and *msbA-KD* (right column; grey cells) co-cultured with *Pae* <sup>$\Delta$ tae1</sup> (a) or *Pae*<sup>inactive</sup> (b) (green cells), and with induced CRISPRi. Green foci in *Pae*<sup>WT</sup> indicate aggregates of GFP-labelled ClpV, which signal H1-T6SS firing events. Red arrow indicates lysed cell. Data shown are merged phase and fluorescent channels. Scale bar: 2 $\mu$ m.